

Research paper

Kinesin-7 CENP-E is essential for chromosome alignment and spindle assembly of mouse spermatocytes

Zhen-Yu She^{a,b,*}, Meng-Fei Xu^{a,b,1}, Sun-Ying Jiang^{a,b}, Ya-Lan Wei^{c,d}

^a Department of Cell Biology and Genetics, The School of Basic Medical Sciences, Fujian Medical University, Fuzhou, Fujian 350122, China

^b Key Laboratory of Stem Cell Engineering and Regenerative Medicine, Fujian Province University, Fuzhou, Fujian 350122, China

^c Fujian Obstetrics and Gynecology Hospital, Fuzhou, Fujian 350011, China

^d Medical Research Center, Fujian Maternity and Child Health Hospital, Affiliated Hospital of Fujian Medical University, Fuzhou, Fujian 350001, China



ARTICLE INFO

Keywords:

Kinesin-7
CENP-E
Spermatocyte
Chromosome
Spindle
Meiosis

ABSTRACT

Genome stability depends on chromosome congression and alignment during cell division. Kinesin-7 CENP-E is critical for kinetochore-microtubule attachment and chromosome alignment, which contribute to genome stability in mitosis. However, the functions and mechanisms of CENP-E in the meiotic division of male spermatocytes remain largely unknown. In this study, by combining the use of chemical inhibitors, siRNA-mediated gene knockdown, immunohistochemistry, and high-resolution microscopy, we have found that CENP-E inhibition results in chromosome misalignment and metaphase arrest in dividing spermatocyte during meiosis. Strikingly, we have revealed that CENP-E regulates spindle organization in metaphase I spermatocytes and cultured GC-2 spd cells. CENP-E depletion leads to spindle elongation, chromosome misalignment, and chromosome instability in spermatocytes. Together, these findings indicate that CENP-E mediates the kinetochore recruitment of BubR1, spindle assembly checkpoint and chromosome alignment in dividing spermatocytes, which finally contribute to faithful chromosome segregation and chromosome stability in the male meiotic division.

1. Introduction

Error-free chromosome segregation is associated with chromosome congression at prometaphase and chromosome alignment at the spindle equator during metaphase. Defects in chromosome alignment result in aneuploidy, genome instability, and birth defects [1,2]. Centromere-associated protein E (CENP-E) is a large plus-end-directed kinesin motor that mediates kinetochore-microtubule attachment and chromosome alignment during cell division [3–6]. CENP-E proteins accumulate at the outer corona of the kinetochore to regulate microtubule capture [7–9]. Furthermore, CENP-E transports monooriented chromosomes toward the spindle equator alongside kinetochore fibers [3,4,10]. Genetic deletion [11,12], gene ablation [13–15], or chemical inhibition of CENP-E's motor domain [16–18] of CENP-E results in chromosome misalignment, metaphase arrest, and mitotic delay during mitosis.

During meiosis, CENP-E proteins localize at the homologous centromeres in primary spermatocytes from late diakinesis to metaphase I [19] and then translocate from the kinetochores to the spindle midzone

at anaphase onset [20]. The similar expression pattern of CENP-E proteins in the outer kinetochore plate and the fibrous corona in both mitosis and meiosis suggests a potentially conserved role of CENP-E in cell division [19,21]. CENP-E inhibition results in chromosome misalignment and missegregation in mouse spermatocytes during meiosis, which finally contribute to chromosomal instability and the formation of the aneuploidy cells [22]. However, detailed mechanisms of CENP-E in male meiotic division remain largely unknown.

Kinetochore functions as a hub for spindle-microtubule interactions and spindle assembly checkpoint signaling [23]. CENP-E interacts with kinetochore-associated checkpoint kinase BubR1 to regulate kinetochore-microtubule attachment [24,25] and the establishment and maintenance of spindle assembly checkpoint [26–28]. Loss-of-function of CENP-E results in the activation or silence of the spindle assembly checkpoint, suggesting that CENP-E is a key component in the spindle assembly checkpoint during mitosis [26–28]. However, the roles of CENP-E in the spindle assembly checkpoint during meiosis remain obscure.

* Corresponding author at: Department of Cell Biology and Genetics, The School of Basic Medical Sciences, Fujian Medical University, Fuzhou, Fujian 350122, China.

E-mail address: zhenyushe@fjmu.edu.cn (Z.-Y. She).

¹ These authors contributed equally to this work.

GSK923295 is an allosteric inhibitor of CENP-E, which strongly suppresses the microtubule-stimulated ATPase activity of CENP-E [17,29]. Biochemical studies have demonstrated that GSK923295 binds to the allosteric pocket near the ATP binding site and locks the motor domain in a rigor microtubule-bound site by blocking inorganic phosphate release in the ATPase cycle [17]. GSK923295 is a specific CENP-E inhibitor that was used in clinical trials as an anticancer molecule [30,31], which also serves as a powerful tool for the functional analyses of CENP-E in cellular and developmental processes [16,18,22,32,33].

In this study, we have revealed the expression patterns of CENP-E in mouse testes. We have shown that CENP-E inhibition led to prolonged metaphase in spermatocytes in seminiferous tubules. CENP-E is required for chromosome alignment and spindle assembly in dividing spermatocytes both *in vitro* and *in vivo*. Furthermore, we found that CENP-E depletion results in spindle elongation, chromosome misalignment, and chromosome instability in spermatocytes. Taken together, our results suggest that CENP-E regulates chromosome alignment and spindle assembly in spermatocytes, which contribute to chromosome stability and integrity in meiosis.

2. Materials and methods

2.1. Animal experiments and ethics

All animal experiments were reviewed and approved by the Institutional Animal Care and Use Committee at Fujian Medical University, China (Protocol No. SYXK 2016-0007). All mouse experiments were performed according to the Guide for the Care and Use of Laboratory Animals of Fujian Medical University and the ARRIVE guidelines. All animal experiments were carried out in accordance with the U.K. Animals (Scientific Procedures) Act, 1986 and associated guidelines, EU Directive 2010/63/EU for animal experiments.

2.2. Reagents and antibodies

Primary antibodies used in this study are listed as follows: rabbit anti-CENP-E polyclonal antibody (Proteintech group, Cat. 28,142-1-AP), mouse anti-CENP-E monoclonal antibody (Santa Cruz Biotechnology, Cat. sc-376,685), rabbit anti-CENP-E polyclonal antibody (Sangon Biotech, Cat. D261553), mouse anti- α -tubulin monoclonal antibody (Abcam, Cat. ab7291), mouse anti- α -tubulin monoclonal antibody (Santa Cruz Biotechnology, Cat. sc-17,788), rabbit anti-TUBA4A polyclonal antibody (Sangon Biotech, Cat. D110022), mouse anti-SYCP3 monoclonal antibody (Santa Cruz Biotechnology, Cat. sc-74,569), rabbit anti-SYCP1 monoclonal antibody (Abcam, Cat. ab175191), rabbit anti- β -tubulin monoclonal antibody (Beyotime, Cat. AF1216), mouse anti-PRC1 monoclonal antibody (Santa Cruz Biotechnology, Cat. sc-367,983), rabbit anti-DDX4/MVH monoclonal antibody (Abcam, Cat. ab270534), rabbit anti- γ H2A.X (phospho S139) monoclonal antibody (Abcam, Cat. ab-81,299), rabbit anti-Histone H3 (phospho S10) monoclonal antibody (Abcam, Cat. ab267372), mouse anti- γ -tubulin monoclonal antibody (Santa Cruz Biotechnology, Cat. sc-17,788), and rabbit anti-BubR1 monoclonal antibody (Abcam, Cat. ab254326), rabbit anti-CDKN1A polyclonal antibody (Sangon Biotech, Cat. D120403), mouse anti-Aurora B monoclonal antibody (Santa Cruz Biotechnology, Cat. sc-374,669). The secondary antibodies used in this study are listed as follows: Alexa Fluor 488-conjugated goat anti-rabbit IgG (H + L) (Beyotime, Cat. A0423), Alexa Fluor 555-conjugated donkey anti-mouse IgG (H + L) (Beyotime, Cat. A0460), Alexa Fluor 488-conjugated goat anti-mouse IgG (H + L) (Beyotime, Cat. A0428), Alexa Fluor 555-conjugated donkey anti-rabbit IgG (H + L) (Beyotime, Cat. A0453).

2.3. Establishment of CENP-E inhibition mouse models

The 3-week-old male ICR mice were purchased from Shanghai SLAC

Laboratory Animal CO. LTD (Shanghai, China). The GSK923295 inhibitor was purchased from MedChemExpress (Cat. HY-10299), dissolved in DMSO at a final concentration of 10 mM, and stored at -80°C . In this study, the concentrations of GSK923295 (the final concentration at 10 μM) were chosen according to previous studies [17,22] and dissolved in PBS, and then injected into mouse testis at a final concentration of 10 μM . In previous studies, we have conducted a series of experiments with multiple concentrations of GSK923295, including 100 nM, 1, 2, 4, 12, and 48 μM , to validate the concentrations, dosages, and duration of GSK923295 inhibition [22,33]. GSK923295 was injected into 3-week-old male ICR mice every three days for a total of two times. Then the testes were harvested for subsequent analyses at the age of 4 weeks. Mice were housed in a pathogen-free facility at Fujian Medical University under the standard environment and exposed to a 12: 12 h light: dark cycle with free access to water and food.

2.4. Cell culture, transfection, and treatment

The GC-2 spd cells (ATCC No. CRL-2196) were obtained from American Type Culture Collection. Cells were cultured in Dulbecco Modified Eagle's Medium/high glucose (Gibco, Cat. C11995500BT) containing 10 % fetal bovine serum (FBS, Every green, Cat. 1101-8611) and 1 % penicillin-streptomycin (Hyclone, Cat. SV30010). Cells were cultured in a humidified incubator (Heal Force, No. HF90/HF240) with 5 % CO_2 at 37°C .

siRNA transfection was performed with Lipofectamine RNAiMAX transfection reagent (Thermo Fisher Scientific, Cat. 13778150) according to the manufacturer's protocols. For gene knockdown, cells were seeded at a 24-well plate and cultured at 70–80 % confluent before siRNA transfection. Two siRNA oligonucleotides targeting *Mus musculus* CENP-E (GenBank accession number NM_173762.4) were synthesized, annealed, and purified according to the manufacturer's instructions (Sangon Biotech). The sequences of RNA oligonucleotides are listed as follows: negative control, 5'-UUCUCCGAACGUGUCACGUTT-3'; CENP-E siRNA-1, 5'-GGAAGAAAGUCAAGAGGAATT-3' and CENP-E siRNA-2, 5'-CUGCUGAACUGGAGAGAAATT-3'. For a 24-well plate, 1 μl Lipofectamine RNAiMAX reagent was diluted into a 25 μl serum-free DMEM medium. And 20 μl 20 μM siRNA was diluted into a 25 μl serum-free DMEM medium. The siRNA and Lipofectamine reagent were mixed and incubated at room temperature for 5 min. The siRNA-lipid complex was added into cells with a final concentration of 200 nM and then incubated at 37°C for 36–48 h as indicated in each figure legend. The efficiency of siRNA knockdown was validated using quantitative real-time PCR analysis and immunohistochemistry experiments.

For the analysis of cell viability, the GC-2 spd cells were grown in a 24-well plate at 50–60 % confluent for 24 h, and then treated with GSK923295 at a final concentration of 10 nM, 50 nM, 400 nM, 1 μM , 5 μM , 12.5 μM , 25 μM and 62.5 μM , respectively. Cells were incubated with GSK923295 at 37°C for 24 h and then digested with 0.25 % trypsin-EDTA (Gibco, Cat. 25200056) at 37°C for 1 min. Cell viability was examined using a CellTiter96 aqueous one solution cell proliferation assay (Promega, Cat. G3580) according to the manufacturer's instructions. Luminescence was determined in a 96-well flat-bottom microplate (Corning, Cat. 3599) at $A_{490\text{nm}}$ using a microplate reader (BioTek, No. 180316F).

2.5. Immunofluorescence and confocal microscopy

For immunofluorescence of the tissues, the 5 μm -thick sections of mouse testes were prepared using an ultra-thin semiautomatic microtome (Leica, No. RM2016). Slides were incubated in xylene for 40 min and then rehydrated in 100 % ethanol for 5 min, in 95 % ethanol for 5 min, in 80 % ethanol for 2 min, and in 70 % ethanol for 2 min. Slides were incubated in distilled water for 5 min and then in 0.1 M PBS for 5 min. For antigen retrieval, the slides were immersed in 10 mM citrate buffer (pH 6.0) and boiled for 5 min using the standard high-pressure

repair method. Slides were incubated with distilled water two times and then with PBST for 5 min. For antigen blocking, slides were incubated with 3 % BSA/PBST at 37 °C for 1 h. Samples were incubated with primary antibodies at 37 °C for 1 h and then at 4 °C for 12 h. After washing with PBST three times, samples were incubated with secondary antibodies at 37 °C for 1 h. After washing with PBST five times, the samples were counterstained with 4', 6-diamidino-2-phenylindole staining solution (DAPI, Beyotime, Cat. 1006) at room temperature for 5 min. Slides were mounted with the anti-fade mounting medium (Beyotime, Cat. P0126).

For immunofluorescence of cultured cells, cells were grown on 12 mm glass coverslips (CITOGLAS) and then fixed in 4 % paraformaldehyde/PBS at room temperature for 10 min. Samples were washed three times with PBS and then incubated with 0.25 % Triton X-100/PBS at room temperature for 10 min. Samples were washed three times with PBS and then blocked with 1 % BSA/PBST at 37 °C for 1 h. Cells were incubated with primary antibodies at 4 °C for 12 h and then washed three times with PBS. Cells were incubated with secondary antibodies at 37 °C for 1 h and then washed five times with PBS. The nuclei were stained with DAPI staining solution (Beyotime, Cat. 1006). Slides were mounted with an anti-fade mounting medium (Beyotime, Cat. P0126).

Images were acquired using a Nikon Ti—S2 microscope (Nikon No. Ti—S2) equipped with a Plan Fluor 40×/NA 0.75 objective; a Plan Fluor 20×/NA 0.40 objective; a Plan Fluor 10×/NA 0.25 objective; a DS-Ri2 camera (Nikon); and 488-nm, 561-nm, and 640-nm solid-state lasers (Nikon No. Intenslight C-HGI). Images were acquired by NIS-Elements imaging software (Nikon) and analyzed by the Image J software (NIH). For high-resolution imaging, images were acquired with a Leica scanning confocal microscope (Leica No. TCS SP8) equipped with an HC PL APO CS2 63×/NA 1.40 objective.

2.6. Hematoxylin-eosin staining and the Giemsa staining

For HE staining, mouse testes were harvested and fixed in 10 % formaldehyde at room temperature for 12 h. The samples were dehydrated in 70 % ethanol for 1 h, in 85 % ethanol for 1 h, in 95 % ethanol for 1 h, and in 100 % ethanol for 1 h. The samples were incubated with xylene for 40 min and then in paraffin for 1 h at 60 °C. The 5 µm-thick sections were prepared using an ultra-thin semiautomatic microtome (Leica RM2016). The slides were incubated in xylene for 40 min, in 100 % ethanol for 6 min, in 95 % ethanol for 2 min, in 90 % ethanol for 2 min, in 80 % ethanol for 2 min, and in 70 % ethanol for 2 min. After washing with distilled water for 5 min, slides were stained with Mayer's hematoxylin solution for 6 min at room temperature. Slides were washed with tap water for 5 min and then incubated with distilled water for 2 min. Slides were incubated with 1 % ethanol hydrochloride for 3 s and then rinsed with tap water for 2 min. The cytoplasm was stained with 1 % eosin for 15 s and then incubate with 95 % ethanol for 5 s, with 100 % ethanol for 2 min, and in xylene for 40 min. Slides were sealed with neutral gum for subsequent analyses.

For the Giemsa staining, cells were fixed with 4 % paraformaldehyde at room temperature for 10 min. Cells were washed three times with PBS and then stained by the Giemsa staining solution supplemented with PBS (pH 6.8) at room temperature for 15 min. Cells were washed three times with distilled water and sealed with 10 % glycerol.

For periodic acid Schiff (PAS) staining, the 5 µm-thick sections were dewaxed with xylene for 40 min, and incubated with gradient ethanol for 2 min, respectively. The slides were rinsed in distilled water for 2 min, then in 1 % periodate aqueous solution for 2 min, and the Schiff reagent staining for 25 min. The slides were incubated with 0.5 % sodium sulfite for 6 min and then rinsed in tap water for 5 min. After incubation with Mayer's hematoxylin solution for 2 min, the slides were washed with tap water and distilled water for 6 min, respectively. The slides were incubated with 95 % and 100 % ethanol for 2 min, respectively. The slides were incubated with xylene and then sealed with

neutral gum.

2.7. Quantitative real-time PCR, gene expression analysis, and Western blot

Total RNAs were extracted using a UNIQ-10 column Trizol total RNA extraction kit (Sangon Biotech, Cat. B511321) according to the manufacturer's protocols. RNA concentrations were determined using an ultraviolet spectrophotometer (Thermo Fisher Scientific, No. NanoDrop 2000c). cDNAs were synthesized using the PrimeScript RT Master Mix (Perfect Real Time) (TaKaRa, Cat. RR036A) according to the manufacturer's protocols. The PCR programs for reverse transcription are listed as follows: 37 °C, 30 min; 85 °C, 5 s; and then at 4 °C, ∞. For gene amplification, the transcripts were amplified using an Ex Taq polymerase (TaKaRa, Cat. RR001B) according to the manufacturer's protocols. The PCR programs for gene amplification are listed as follows: 98 °C, 10 s; 98 °C, 10 s, 55 °C, 30 s, 72 °C, 60 s for 32 cycles; 72 °C, 10 min; and then at 4 °C, ∞. The primers were listed as follows: *CENP-E* F1, 5'-GTGAAGGCCGAGCTTTCTCA-3'; *CENP-E* R1, 5'-GTCCTTACCACCACAAGCA-3' (*M. musculus CENP-E* GenBank accession No. NM_173762.4). *β-Actin* F1, 5'-CCCTGAACCCTAAGGCCA-3'; *β-Actin* R1, 5'-CCACAGGATCCATACCCAAG-3' (*M. musculus Actin* GenBank accession No. NM_007393.5). The *β-Actin* gene served as a loading control.

For quantitative real-time PCR, the mixture of template DNA, forward and reverse primers, and SYBR Green qPCR Mix (Beyotime, Cat. D7265) were prepared according to the manufacturer's protocols. The PCR programs for quantitative real-time PCR are listed as follows: 95 °C, 2 min; 95 °C, 15 s, 60 °C, 30 s for 40 cycles; for the analysis of melting curve, 95 °C, 15 s, 60 °C, 15 s and 95 °C, 15 s. The PCR programs were performed using an AriaMx Real-Time PCR instrument (Agilent Technologies, No. AriaMx G8830-64001). The results were acquired using a standard Aria software (Agilent software) and analyzed using the Microsoft Excel 2013 and GraphPad Prism version 6 software (GraphPad Software). $\Delta\Delta C_t$ values were used to quantify relative expression levels of target genes. The specific primers were designed using the NCBI Primer-Blast software (www.ncbi.nlm.nih.gov/tools/primer-blast/) and were listed in Supplemental Table S1.

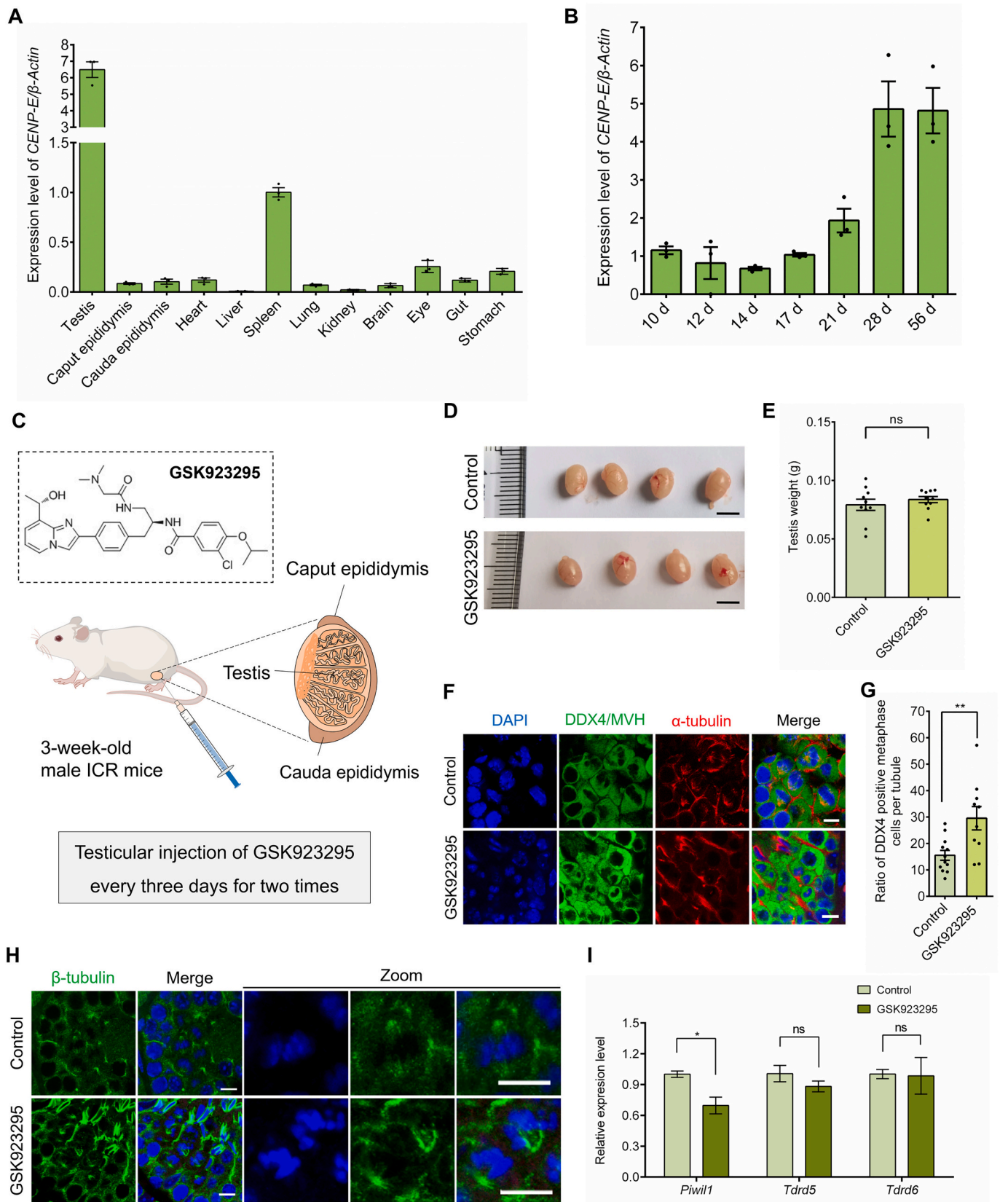
For western blot, total proteins of the GC-2 spd cells were extracted with the RIPA lysis buffer. Proteins were separated by 8 % polyacrylamide gels and were transferred onto polyvinylidene difluoride (PVDF) membranes (GE, Cat. 10,600,023) for 3 h. After being blocked for 2 h in QuickBlock blocking buffer (Beyotime, Cat. P0252FT), the PVDF membrane was washed with TBST two times and incubated with primary antibodies for 12 h at 4 °C. The membrane was washed with PBST and incubated for 2 h with HRP-conjugated goat anti-rabbit IgG (Sangon Biotech, Cat. D110058, 1:2000). The protein bands were visualized using the BeyoECL Moon kit (Beyotime, Cat. P0018FS), and were recorded using a ChemiDoc Touch Imaging System (Bio-Rad).

2.8. TUNEL assay

For cell apoptotic analyses, the samples were analyzed using the one-step TUNEL apoptosis assay (Beyotime, Cat. C1086) according to the manufacturer's protocol. Samples were treated with 20 ng/ml DNase-free proteinase K (Sangon Biotech, Cat. B600452) at 37 °C for 30 min. After washing four times with PBS, samples were stained with fluorescein isothiocyanate (FITC)-conjugated dUTP using the TdT-mediated dUTP nick-end labeling method at 37 °C for 60 min. After washing with PBS four times, the nuclei were stained with the DAPI solution for 5 min. The slides were mounted with the anti-fade mounting medium and observed using a Nikon Ti—S2 fluorescent microscope.

2.9. Flow cytometry and cell cycle analysis

For cell cycle analysis of mouse spermatogenic cells, the testes were



(caption on next page)

Fig. 1. Construction of GSK923295-mediated CENP-E inhibition mouse model and gene expression patterns of *CENP-E* gene. (A) Quantitative real-time PCR analyses of expression levels of *CENP-E* in multiple tissues. From left to right, the testis, caput epididymis, cauda epididymis, heart, liver, spleen, lung, kidney, brain, eye and gut were shown. β -Actin was served as the loading control. (B) Quantitative real-time PCR analyses of expression levels of the *CENP-E* gene in the developing testes at different developmental stages, including the testes from the mice at the age of 10, 12, 14, 17, 21, 28, and 56 days. β -Actin was served as the loading control. (C) Construction of the CENP-E inhibition mouse model by testicular injection of GSK923295 at a final concentration of 10 μ M. The inhibitor was injected into 3-week-old male ICR mouse testes every three days for two times. (D) Morphology of the testes in the control and GSK923295 groups. Scale bar, 5 mm. (E) Statistical analyses of testis weights in the control and GSK923295 groups were shown. Control, 0.792 ± 0.005 g; GSK923295, 0.837 ± 0.003 g. (F) Representative immunofluorescence images of DDX4/MVH and α -tubulin in the control and GSK923295 groups. α -tubulin, red; DDX4/MVH, green; DAPI, blue. Scale bar, 10 μ m. (G) Ratios of DDX4/MVH positive metaphase cells per seminiferous tubule were shown. Control, 15.52 ± 1.87 %; GSK923295, 29.54 ± 4.42 %, $N = 1109$, Group = 12. (H) Representative immunofluorescence images of spindle microtubules in metaphase I spermatocytes in the control and GSK923295 groups. The enlarged images were shown in the zoom. α -tubulin, green; DAPI, blue. Scale bar, 10 μ m. (I) Quantitative real-time PCR analyses of expression levels of *Ptwill1*, *Tdrd5*, and *Tdrd6* genes in the testes of the control and GSK923295 groups. For all graphs, student's *t*-test. Error bars, mean \pm SEM. ns, $p > 0.05$; *, $p < 0.05$; **, $p < 0.01$. (For interpretation of the references to colour in this figure legend, the reader is referred to the web version of this article.)

cut into pieces using surgical scissors and then digested using 0.25 % trypsin-EDTA at 37 °C for 20 min. For cell cycle analysis of the GC-2 spd cells, cells were harvested 0.25 % trypsin-EDTA at 37 °C for 1 min. Samples were centrifuged at 1000 \times g for 5 min. Samples were washed with PBS for 5 min and then centrifuged at 1000 \times g for 5 min. Samples were fixed in 70 % cold ethanol at 4 °C overnight. Samples were stained with propidium iodide (PI) staining solution (0.1 % Triton X-100/PBS, 20 μ g/ml RNase A and 50 μ g/ml PI; Beyotime, Cat. C1052) at 37 °C for 1 h. Cell cycle analysis was carried out using a flow cytometer (BD, FACSCanto™ II) and the Modfit LT32 software (Verity Software House).

2.10. Statistical analysis

All experiments were repeated at least three times. Data were shown as the mean \pm SEM. The sample size was indicated in each figure legend. The stages of seminiferous tubules in mouse testes were defined by the groups of spermatogenic cells according to the standard guidelines [34–36]. Fluorescence intensities and the degree of colocalization were analyzed using line scan analyses of the Image J software (NIH). For comparisons of two groups, statistical significance was tested using the unpaired student's *t*-test using the GraphPad Prism version 6 (GraphPad Software). For comparisons of multiple groups (more than two groups), the ANOVA Dunnett's multiple comparisons test was applied using the GraphPad Prism software as indicated in figure legends. *P* values and the number of experiments used for the quantifications are indicated in each figure legend. ns, not significant; *, $P < 0.05$; **, $P < 0.01$; ***, $P < 0.001$. The investigators were blinded to the group allocation during the experiment and/or when assessing the outcome. Simple randomization was applied in the sample analysis and mouse experiments.

3. Results

3.1. Expression patterns of *CENP-E* gene in the developing testes and the construction of the GSK923295-mediated *CENP-E* inhibition mouse model

Firstly, we examined expression levels of the *CENP-E* gene in different tissues of 8-week-old mice using quantitative real-time PCR analyses, including the testis, caput epididymis, cauda epididymis, heart, liver, spleen, lung, kidney, brain, eye, gut and, stomach (Fig. 1A; Fig. S1A). Notably, we found that the *CENP-E* gene was highly expressed in mouse testes compared with other organs (Fig. 1A; Fig. S1A). In addition, the *CENP-E* gene was also highly expressed in the spleen tissue (Fig. 1A; Fig. S1A). To investigate expression patterns of the *CENP-E* gene at different stages of spermatogenesis, we performed quantitative real-time PCR to analyze expression levels of the *CENP-E* gene in mouse testes at the age of 10, 12, 14, 17, 21, 28, and 56 days, respectively (Fig. 1B; Fig. S1B). We found that the *CENP-E* gene was expressed throughout the process of mouse spermatogenesis from the age of 10–56 days. *CENP-E* gene was expressed in mouse testes from 10 days to 21 days after birth, significantly increased from 21 days after birth to 28 days after birth, and remained at a relatively high level from 28 days to

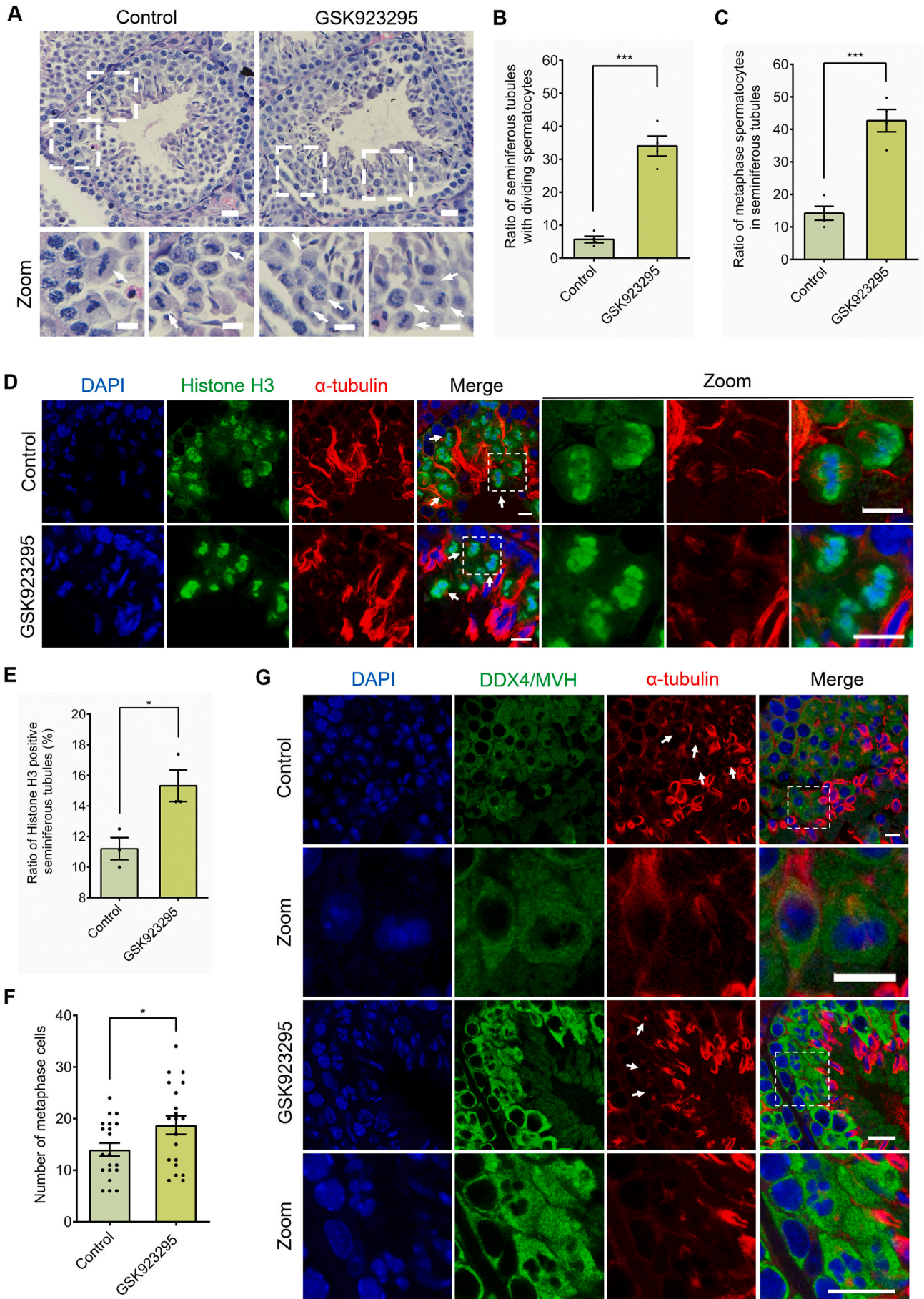
56 days (Fig. 1B; Fig. S1B). Our results have revealed the expression patterns of the *CENP-E* gene in mouse developing testes, which indicates a potential role of CENP-E in spermatogenesis.

To further study the developmental roles of CENP-E proteins in testes, we constructed a CENP-E inhibition mouse model. We took advantage of the specific CENP-E inhibitor GSK923295, which binds CENP-E's motor domain, inhibits the ATPase activity, and locks CENP-E motors on microtubules [17,29]. The allosteric inhibitor GSK923295 was injected into 3-week-old male ICR mice every three days two times. The testes were harvested for subsequent analyses at the age of 4 weeks (Fig. 1C). The morphology of mouse testes in the control and GSK923295 groups did not show obvious defects after GSK923295 injection (Fig. 1D). There was no significant difference between the weights of the testes in the control and GSK923295 groups (Fig. 1E; Fig. S1C). These results suggest that the injection of GSK923295 is suitable for the construction of the CENP-E inhibition mouse model.

To further investigate the functions of CENP-E in mouse spermatogenesis, we used the DDX4/MVH (also referred to as mouse VASA homolog, MVH) antibody, an ATP-dependent RNA helicase required for spermatogenesis [37,38], for immunostaining of male germ cells. We found that DDX4/MVH-positive metaphase cells in seminiferous tubules were significantly increased after CENP-E inhibition (Fig. 1F, G). The results of immunostaining of β -tubulin or Histone H3 (phospho S10), a marker of condensed chromosomes during late G₂ and metaphase, also showed an increased population of metaphase spermatocytes in the GSK923295 group (Fig. 1H; Fig. S1D). Gene expression analyses indicated that the expression level of *Ptwill1*, a marker of prophase I of meiosis, was slightly decreased after CENP-E inhibition (Fig. 1I). There were no significant changes in the expression levels of *Tdrd5* and *Tdrd6* in the control and GSK923295 groups (Fig. 1I). Furthermore, we observed that there were no significant differences between the control and GSK923295 groups in the expression levels of genes encoding synaptonemal complex protein 3 (*Sycp3*) [39], *Rec8* meiotic recombination protein (*Rec8*) [40,41], DNA meiotic recombinase 1 (*Dmc1*) [42] and kinesin family member 11 (*Eg5*) [33], which are marker genes of early to mid-prophase I (Fig. S1E). Early round spermatids express genes encoding regulatory factor X, 2 (*Rfx2*) [2], cAMP responsive element modulator (*Crem*) [43], and *SRY* (sex determining region Y)-box 30 (*Sox30*) [44] transcription factors, which are key genes involved in the processes of spermiogenesis. And there were no differences between the control and GSK923295 groups in the expression of *Rfx2*, *Crem*, and *Sox30* genes (Fig. S1F). In addition, there was an increase in the expression level of Spermatid nuclear transition protein 1 (*Tnp1*) and Protamine-2 (*Prm2*) (Fig. S1F), which are key genes in the compaction of the haploid genome in late round spermatids [45,46].

3.2. *CENP-E* inhibition resulted in prolonged metaphase in spermatocytes

To further study the roles of CENP-E in spermatogenesis, we performed HE staining to examine the phenotypes of seminiferous tubules after CENP-E inhibition by GSK923295 injection. We found that CENP-E inhibition resulted in the increase of dividing spermatocytes at stage XII



(caption on next page)

Fig. 2. CENP-E inhibition led to the disruption of spermatogenic wave and metaphase arrest of dividing spermatocytes. (A) Representative images of HE staining of seminiferous tubules in the control and GSK923295 groups. Scale bar, 20 μm . The arrow indicates the metaphase-arrested spermatocytes. The enlarged image of the dashed box was shown in the zoom. In the zoom, scale bar, 10 μm . (B) Ratios of seminiferous tubules with dividing spermatocytes in the control and GSK923295 groups. Control, $5.66 \pm 0.98\%$, $N = 4$; GSK923295, $34.03 \pm 3.04\%$, $N = 4$. (C) Ratios of metaphase spermatocytes in seminiferous tubules of the control and GSK923295 groups. Control, $14.21 \pm 2.14\%$, $N = 4$; GSK923295, $42.70 \pm 3.45\%$, $N = 4$. (D) Immunofluorescence images of Histone H3 and α -tubulin in the control and GSK923295 groups. α -tubulin, red; Histone H3, green; DAPI, blue. Scale bar, 10 μm . The enlarged box was shown in the zoom. The arrow indicates the metaphase I spermatocytes. (E) Ratios of Histone H3 positive seminiferous tubules in the control and GSK923295 groups. Control, $11.20 \pm 0.72\%$; GSK923295, $15.32 \pm 1.03\%$, $N = 89$; Group = 3. (F) Relative number of metaphase cells in each seminiferous tubule of the control and GSK923295 groups. Control, 14.00 ± 0.27 , $N = 555$; Group = 29. GSK923295, 18.75 ± 1.80 , $N = 375$; Group = 20. (G) Immunofluorescence images of DDX4/MVH and α -tubulin in the control and GSK923295 groups. α -tubulin, red; DDX4/MVH, green; DAPI, blue. Scale bar, 10 μm . For all graphs, student's *t*-test. Error bars, mean \pm SEM. *, $p < 0.05$; ***, $p < 0.001$. (For interpretation of the references to colour in this figure legend, the reader is referred to the web version of this article.)

of seminiferous tubules (Fig. 2A). Statistical analyses suggested that the ratios of seminiferous tubules with dividing spermatocytes significantly increased from 5.66 % in the control group to 34.03 % in the GSK923295 group (Fig. 2B). Moreover, the ratios of metaphase spermatocytes in total spermatocytes of each seminiferous tubule significantly increased to 42.70 % after CENP-E inhibition compared with 14.21 % in the control group (Fig. 2C). In addition, we stained the seminiferous tubules using the PAS staining and classified the stages of each tubule according to the standard guidelines [34–36]. We found that the ratio of each stage of seminiferous tubules was not significantly influenced after CENP-E inhibition compared with the control group (Fig. S2A–D). These results indicate that CENP-E inhibition leads to cell cycle arrest of spermatocytes at metaphase in mouse testes.

To validate these results, we performed immunofluorescence to stain Histone H3 (phospho S10) and α -tubulin (Fig. 2D). We observed that Histone H3-positive spermatocytes substantially increased after CENP-E inhibition (Fig. 2D). The ratios of Histone H3-positive seminiferous tubules increased to 15.32 % compared with 11.20 % in the control group (Fig. 2E). Furthermore, the number of Histone H3-positive metaphase cells significantly increased after CENP-E inhibition (Fig. 2F). These results indicate that CENP-E inhibition led to the G₂/M arrest and prolonged metaphase in spermatocytes.

We then used a germ cell marker ATP-dependent RNA helicase DDX4 to stain the germ cells. We found that CENP-E inhibition results in chromosome misalignment in primary spermatocytes (Fig. 2G). We next examined whether the cell cycle was elongated in prophase I using the immunostaining of γ -H2AX, a marker protein of double-strand DNA breaks and sex chromosomes (Fig. S3A). We found that the number of γ -H2AX in each seminiferous tubule increased after CENP-E inhibition (Fig. S3B), which indicating DNA double-strand breaks were formed but not completely repaired after CENP-E inhibition.

To examine whether CENP-E inhibition led to cell cycle arrest and finally resulted in apoptosis, we performed the TUNEL staining to label the apoptotic cells in seminiferous tubules (Fig. S3C). We quantified the apoptotic cells in each seminiferous tubule and found that there were no significant differences between the control and GSK923295 groups (Fig. S3D). Furthermore, we performed flow cytometry using Annexin V and PI staining to examine the apoptosis in testicular cells of the control and GSK923295 groups (Fig. S3E–I). Consistent with the TUNEL analyses, we observed that the ratios of Annexin V⁺/PI⁻ cells, the apoptotic cells, did not increase after CENP-E inhibition (Fig. S3E–I). These results indicate that GSK923295 mediated CENP-E inhibition did not result in obvious cell apoptosis in mouse testis.

3.3. CENP-E inhibition led to spindle assembly defects and chromosome misalignment in primary spermatocytes

To examine spindle microtubules in dividing primary spermatocytes, we performed immunostaining of tubulin alpha-4A chain (TUBA4A) and protein regulator of cytokinesis 1 (PRC1), a marker of antiparallel microtubules in cell division (Fig. 3A). Notably, we found that the PRC1-labelled microtubules were organized in wild-type metaphase I spermatocytes (Fig. 3A). However, the PRC1-labelled microtubules became less and disorganized after CENP-E inhibition (Fig. 3A). We then

quantified the stretches of PRC1 in each spermatocyte and found that there was a decrease in the stretches of the PRC1-labelled spindle microtubules in metaphase I spermatocytes (Fig. 3B). Line-scan analyses of fluorescent intensities of PRC1 and spindle microtubules also showed that the PRC1-labelled microtubules were disrupted after CENP-E inhibition (Fig. 3C, D).

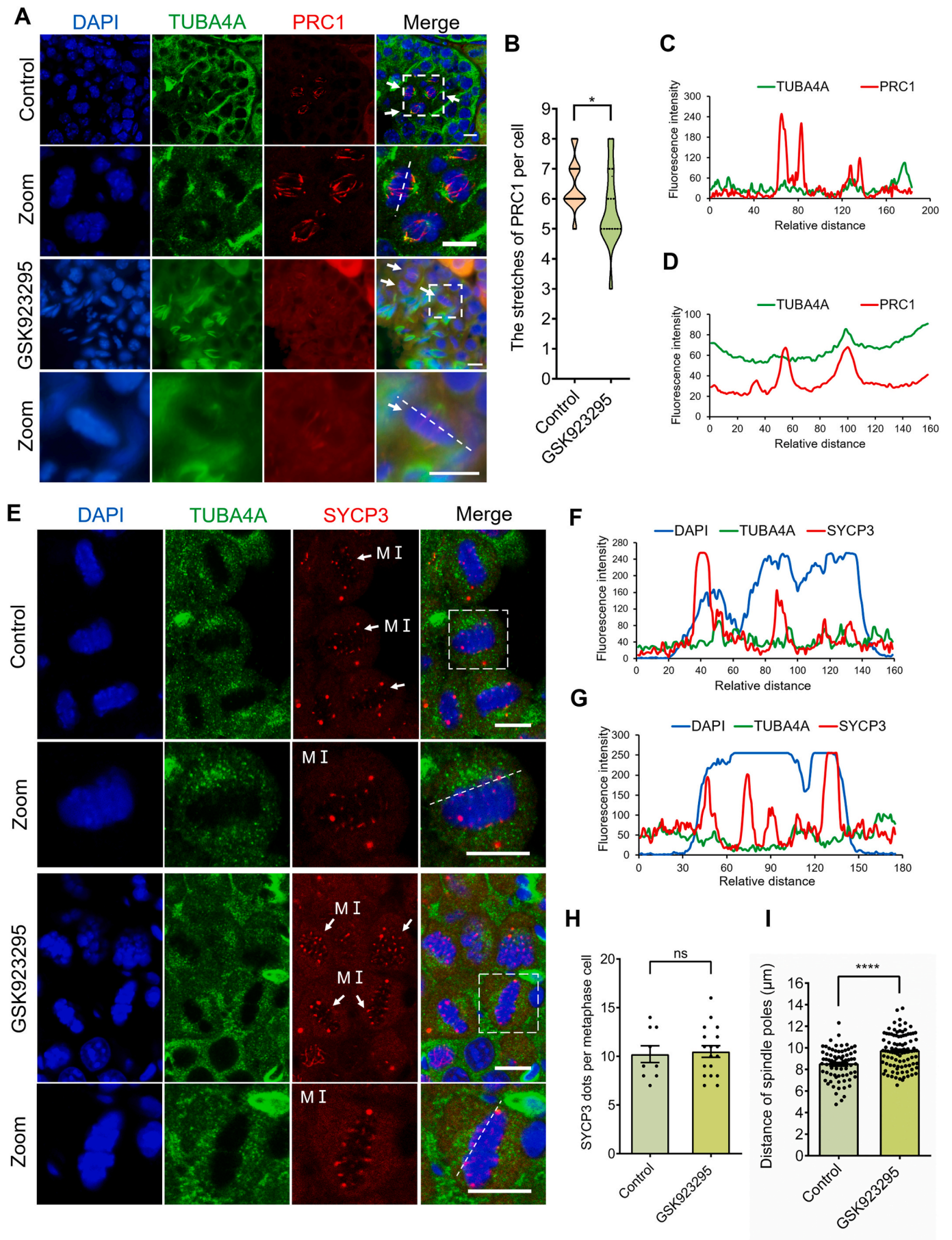
Furthermore, we performed immunofluorescence to label the centromeres using the SYCP3 antibody, a component of the synaptonemal complexes required for centromere pairing in male germ cells during meiosis [47,48] (Fig. 3E). The centromeres in dividing primary spermatocytes were not disrupted in the GSK923295 group compared with the control group (Fig. 3F–H). The quantifications of SYCP3 dots per metaphase cell showed that there were no significant changes in the SYCP3-labelled centromeres in metaphase I spermatocytes of the control and GSK923295 groups (Fig. 3H).

We then used immunofluorescence to stain the transverse filament of synaptonemal complexes using the synaptonemal complex protein 1 (SYCP1) antibody (Fig. S4A). We found that there were no significant changes in SYCP1 stretches per cell in the control and GSK923295 groups (Fig. S4B). Furthermore, we found that SYCP3 stretches per cell were not influenced in the GSK923295 group compared with the control group (Fig. S4C–D).

3.4. CENP-E is essential for the regulation of the spindle length in spermatocytes

Quantifications of the distance of spindle poles in metaphase spermatocytes revealed that the length of spindle microtubules was $9.71 \pm 0.16 \mu\text{m}$ in the GSK923295 group compared with $8.48 \pm 0.17 \mu\text{m}$ in the control group (Fig. 3I). Strikingly, we found that CENP-E inhibition resulted in the elongation of spindle microtubules compared with the regular spindle microtubules in the control group (Fig. 3E, I and Fig. 4A). We also examined the morphology of spindle microtubules in secondary spermatocytes using immunofluorescence of TUBA4A and SYCP3 (Fig. 4A–D). The number of SYCP3-positive cells per seminiferous tubules was not influenced after CENP-E inhibition (Fig. 4A–D).

To further study the mechanisms of CENP-E in dividing spermatocytes, we selected the spermatogenic cell line GC-2 spd (ts), which was derived from 6-week-old mouse testes and transfected with the *simian virus 40 large tumor antigen* gene and a temperature-sensitive mutant of the *p53* tumor suppressor gene [49,50]. The GC-2 spd cells can not differentiate and remain at a premeiotic stage, which provides a useful model cell line for cell division of dividing spermatocytes *in vitro* [49,52]. There is evidence that this cell line has some meiosis-like properties. The kinetic of microtubule assembly is conserved among the GC-2 spd cells and the spermatocytes *in vivo* [49–51]. We synthesized two specific CENP-E siRNA and transfected the siRNA into the GC-2 spd cells for 48 h, respectively. The efficiency of CENP-E-specific siRNA knockdown was validated using the quantitative real-time PCR, immunofluorescence, and the rescue experiments (Figs. S5A, B, C; S6). CENP-E knockdown led to metaphase arrest in the GC-2 spd cells (Fig. S5B). We found that CENP-E knockdown also led to the elongation of spindle poles in the cultured GC-2 spd cells (Fig. 4E; Fig. S5C). Quantifications of the distances of spindle poles in spermatocytes



(caption on next page)

Fig. 3. CENP-E inhibition results in the increase of metaphase I spermatocytes and the disorganization of spindle microtubules. (A) Immunofluorescence images of PRC1 and TUBA4A in the control and GSK923295 groups. PRC1, red; TUBA4A, green; DAPI, blue. Scale bar, 10 μ m. The enlarged box was shown in the zoom. (B) The number of the stretches of PRC1-labelled spindle microtubules per cell. Control, 6.46 ± 0.14 , $N = 35$; GSK923295, 5.67 ± 0.33 , $N = 16$. (C, D) Line-scan analyses of fluorescent intensities of TUBA4A and PRC1 in metaphase I spermatocytes of the control group (C) and the GSK923295 group (D). PRC1, red; TUBA4A, green. The X axis indicates relative distance. The Y axis indicates fluorescent intensities. (E) Immunofluorescence images of SYCP3 and TUBA4A in the control and GSK923295 groups. SYCP3, red; TUBA4A, green; DAPI, blue. Scale bar, 10 μ m. (F, G) Line-scan analyses of fluorescent intensities of SYCP3 and TUBA4A in metaphase I spermatocytes of the control group (F) and the GSK923295 group (G). SYCP3, red; TUBA4A, green; DAPI, blue. (H) The analysis of SYCP3 dots per metaphase I spermatocyte in the control and GSK923295 groups. Control, 1.22 ± 0.86 , $N = 9$; GSK923295, 10.50 ± 0.59 , $N = 18$. (I) The analysis of the distance of spindle poles in metaphase I spermatocytes in the control and GSK923295 groups. Control, 8.48 ± 0.17 μ m, $N = 73$; GSK923295, 9.71 ± 0.16 μ m, $N = 96$. For all graphs, student's *t*-test. Error bars, mean \pm SEM. ns, $p > 0.05$; *, $p < 0.05$; ****, $p < 0.0001$. (For interpretation of the references to colour in this figure legend, the reader is referred to the web version of this article.)

indicated that the spindle length is 8.09 ± 0.27 μ m in the control group, while the spindle length was significantly increased to 10.42 ± 0.43 μ m in the siCENP-E-1 group and 9.41 ± 0.48 μ m in the siCENP-E-2 group (Fig. 4F). Furthermore, we observed that a portion of chromosomes was misaligned and cannot locate at the equatorial plate in the GC-2 spd cells at metaphase (Fig. 4E).

To further validate the roles of CENP-E in spindle length regulation, we treated the GC-2 spd cells with a series of concentrations of GSK923295, including 400 nM, 1 μ M and 5 μ M. We labelled spindle microtubules using immunofluorescence with the α -tubulin antibody. Consistent with the results in the siRNA knockdown group, we found that GSK923295 mediated CENP-E inhibition resulted in the increase of the distances of spindle poles in the GC-2 spd cells (Fig. 5A, B). The distances of spindle poles increased into 10.48 ± 0.23 μ m in the presence of 400 nM GSK923295, and significantly increased to 11.61 ± 0.23 μ m in the presence of 5 μ M GSK923295 compared with 9.60 ± 0.32 μ m in the control group (Fig. 5B). These results suggest that GSK923295-mediated CENP-E inhibition also results in the elongation of spindle length and shows a pattern that the spindle pole distances increase with the increase of the inhibition degree.

3.5. CENP-E depletion resulted in chromosome misalignment, multinuclei, and micronuclei in spermatocytes

We found that CENP-E knockdown led to chromosome misalignment in the GC-2 spd cells. In the GSK923295 group, a portion of chromosomes failed to align at the metaphase plate (Fig. 5C). The GC-2 spd cells with misaligned chromosomes increased to 67.88 % in the siCENP-E-1 group and 50.55 % in the siCENP-E-2 group, compared with 11.93 % in the control group (Fig. 5D). Meanwhile, the cells with multinuclei also slightly increased after CENP-E ablation (Fig. 5E). The cells with abnormal nuclei and micronuclei also slightly increased in the absence of CENP-E (Fig. 5F, G).

Consistent with the results in cultured GC-2 spd cells, we also observed that homologous chromosomes were misaligned in seminiferous tubules after CENP-E inhibition in mouse testes (Fig. 6A). The spindle organization in metaphase I spermatocytes was also disrupted after CENP-E inhibition (Fig. 6A). In the GC-2 spd cells, siRNA-mediated CENP-E depletion led to spindle disorganization and multipolar spindles (Fig. 6B). The ratios of disorganized spindles were significantly increased after CENP-E knockdown (Fig. 6C). Similarly, GSK923295-mediated CENP-E inhibition also led to defects in chromosome alignment and spindle organization (Fig. 6D). Furthermore, the cells with abnormal spindles were increased after CENP-E inhibition (Fig. 6E). Loss-of-function of CENP-E is associated with chromosome misalignment, abnormal spindle, and multipolar spindle in spermatocytes (Fig. 6F).

We found that CENP-E inhibition caused metaphase arrest in the GC-2 spd cells (Fig. S7A). CENP-E inhibition also led to the decreased cell viability in the GC-2 spd cells, especially in the presence of GSK923295 from the concentrations at 5 to 62.5 μ M (Fig. S7B). The Giemsa staining showed that relative cell numbers were decreased and the metaphase-arrested cells significantly increased after CENP-E inhibition (Fig. S7C-E). Cell colony assays showed that the formation of cell colony was not

affected in the 400 nM GSK923295 group, while was significantly suppressed in the 2 μ M and 10 μ M GSK923295 groups (Fig. S7F, G). Furthermore, we observed that the GC-2 spd cells grew slower compared with the wild-type cells (Fig. S7H), while in the 400 nM group, the GC-2 spd cells grew slightly faster than the wild-type cells, and in the 6 μ M group (Fig. S7I).

3.6. Chromosome stability and genome integrity were mediated by CENP-E

We further analyzed chromosome stability in the GC-2 spd cells using a series of concentrations of GSK923295, including 400 nM, 1 μ M, 5 μ M, and 12.5 μ M (Fig. S8). We observed that metaphase-arrested GC-2 spd cells significantly increased in the GSK923295 group (Fig. S8A-B). We found that CENP-E inhibition resulted in the increase of multinucleated cells into 8.64–15.77 % compared with 3.16 % in the control group (Fig. S8C). Moreover, there was a significant increase in the abnormal nucleus and micronucleus after CENP-E inhibition (Fig. S8D, E). Flow cytometry analyses revealed that there was a significant increase in the G₂-M phase cells after CENP-E inhibition for 24 or 48 h in cultured GC-2 spd cells (Fig. S8F-K). Meanwhile, there is a decrease in the G₀-G₁ phase cells after CENP-E inhibition in cultured GC-2 spd cells (Fig. S8G). The populations of subdiploid cells and multiploid cells were increased after CENP-E inhibition (Fig. S8J, K).

To examine the consequences of CENP-E inhibition in spermatogenic cells *in vivo*, we performed flow cytometry to examine the populations of spermatogenic cells in mouse testes (Fig. 7A). We found that the ratios of the haploid cells were not significantly influenced in the GSK923295 group compared with the control group (Fig. 7B). Notably, we found that the diploid cells significantly decreased to 18.22 ± 0.63 % in the GSK923295 groups compared with 24.58 ± 1.90 % in the control group (Fig. 7C). Furthermore, the tetraploid cells increased from 28.14 ± 1.76 % in the GSK923295 groups compared with 16.42 ± 1.33 % in the control group (Fig. 7D). The ratio of aneuploid cells increased from 13.07 ± 0.75 % to 19.32 ± 0.92 % after CENP-E inhibition (Fig. 7E). These results indicate that CENP-E inhibition causes a decrease in diploid cell populations and an increase in aneuploid and tetraploid cell populations in seminiferous tubules.

Furthermore, we examined the expression patterns of cell cycle-related genes in the control and GSK923295 groups. Quantitative real-time PCR analyses have revealed that expression levels of *Cdk1*, *Mad1*, *Mad2*, *Cdkn1a*, *Aurora A*, and *Plk1* were significantly increased in mouse testes after CENP-E inhibition (Fig. 7F, G). Moreover, the expression level of *BubR1*, *Bub1*, and *Incenp* were significantly decreased in mouse testes after CENP-E inhibition (Fig. 7F, G). The expression level of *Cdc20*, *Cdc25a*, *Cdc25c*, *Wee1*, and *Apc1* genes were not influenced in the testes of the control and GSK923295 groups (Fig. 7F, G).

To further investigate the functions of CENP-E in the spindle assembly checkpoint during meiosis I, we stained the metaphase I spermatocytes with the anti-BubR1 antibody. We found that GSK923295-mediated CENP-E inhibition resulted in the decreased localization of BubR1 proteins at the kinetochores (Fig. 8A). In the control group, BubR1 proteins were accumulated at the kinetochores of aligned chromosomes in the primary spermatocyte during metaphase I. However, a

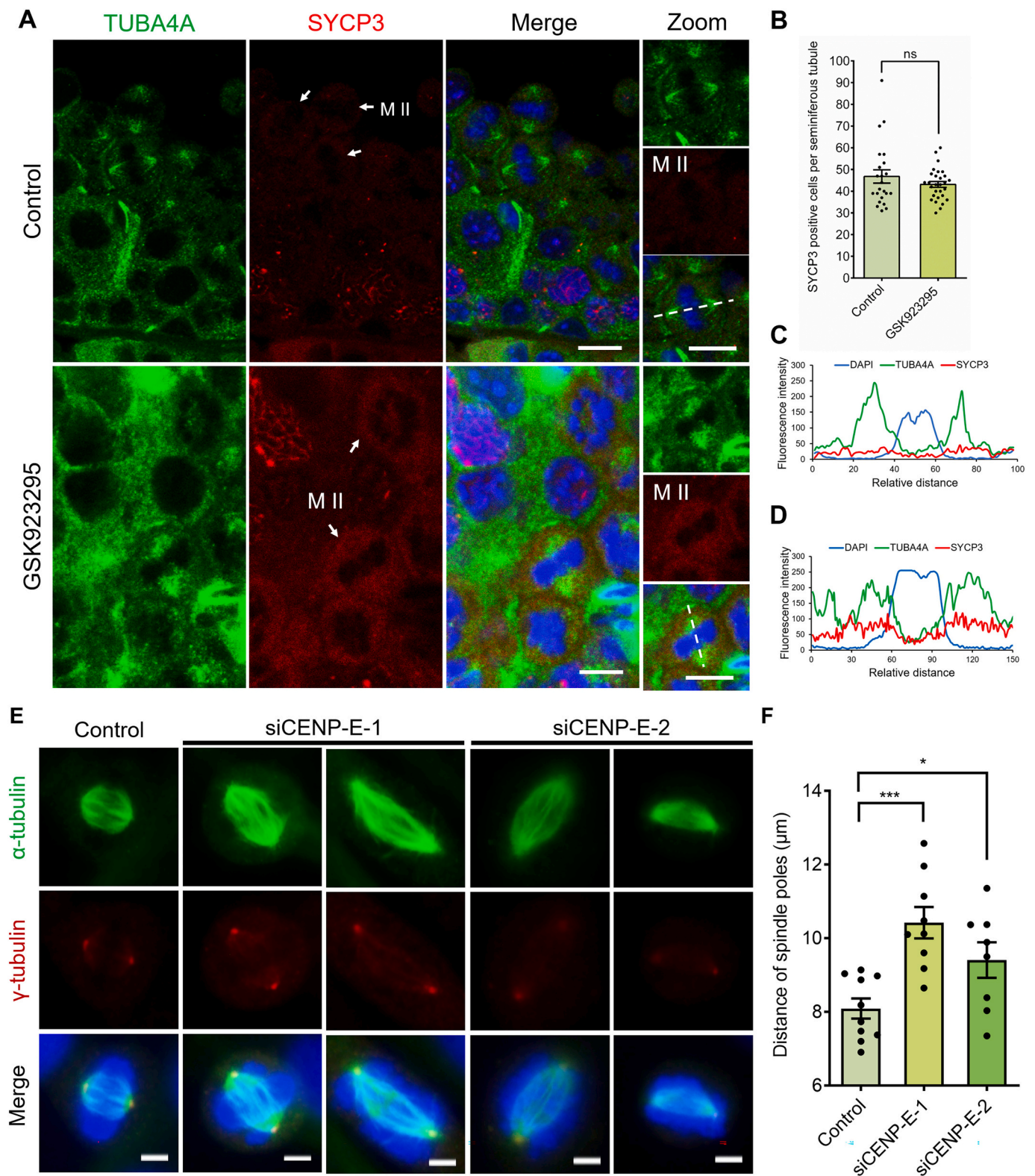
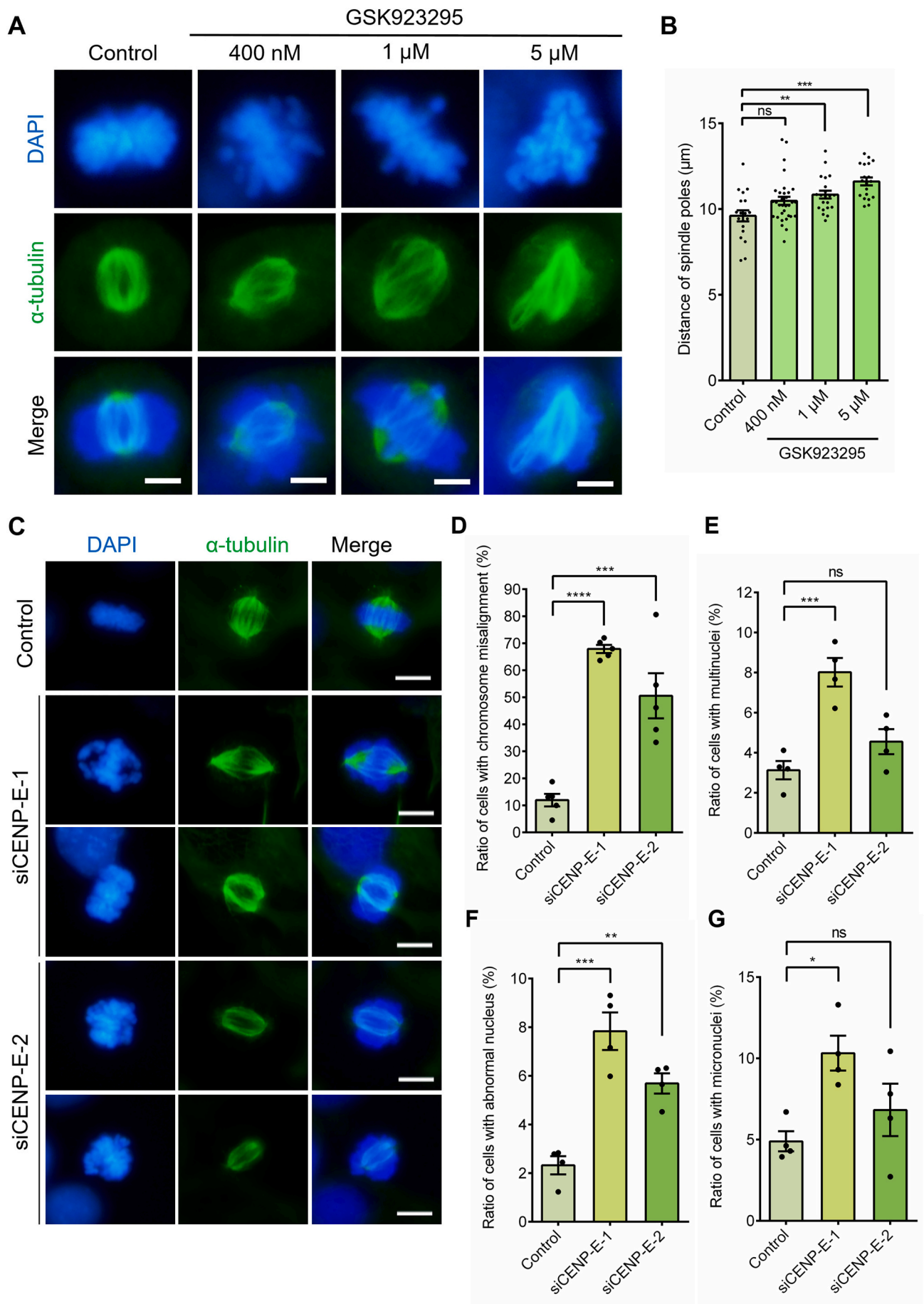


Fig. 4. CENP-E ablation resulted in the elongation of spindle poles and spindle disorganization in dividing spermatocytes. (A) Immunofluorescence images of TUBA4A and SYCP3 in the control and GSK923295 groups. SYCP3, red; TUBA4A, green; DAPI, blue. Scale bar, 10 μm . The indicated spermatocytes were shown in the zoom. (B) The analysis of SYCP3 positive cells per seminiferous tubule in the control and GSK923295 groups. Control, 46.78 ± 3.07 , $N = 23$; GSK923295, 43.10 ± 1.35 , $N = 29$. In this graph, student's *t*-test. (C, D) Line-scan analyses of fluorescent intensities of TUBA4A and SYCP3 in metaphase I spermatocytes of the control group (C) and the GSK923295 group (D). SYCP3, red; TUBA4A, green; DAPI, blue. (E) siRNA-mediated CENP-E knockdown resulted in the elongation of spindle poles in cultured GC-2 spd cells after treatment with siRNA for 48 h. A non-specific negative control siRNA served as the control group. γ -tubulin, red; α -tubulin, green; DAPI, blue. Scale bar, 5 μm . (F) The analysis of the distance of spindle poles in cultured GC-2 spd cells in the control, siCENP-E-1, and siCENP-E-2 groups. Control, 8.09 ± 0.27 μm ; siCENP-E-1, 10.42 ± 0.43 μm ; siCENP-E-2, 9.41 ± 0.48 μm . $n = 10, 9, 8$. Student's *t*-test. For all graphs, error bars, mean \pm SEM. ns, $p > 0.05$; *, $p < 0.05$; ***, $p < 0.001$. (For interpretation of the references to colour in this figure legend, the reader is referred to the web version of this article.)



(caption on next page)

Fig. 5. GSK923295-mediated CENP-E inhibition resulted in increased distances between two spindle poles in cultured GC-2 spd cells. (A) Immunofluorescence images of the spindle microtubules of the GC-2 spd cells in the control and GSK923295 groups. DAPI, blue; α -tubulin, green. Scale bar, 5 μ m. (B) Distances of two spindle poles of the GC-2 spd cells in the control and GSK923295 groups. Control, $9.60 \pm 0.32 \mu$ m; 400 nM, $10.48 \pm 0.23 \mu$ m; 1 μ M, $10.84 \pm 0.23 \mu$ m; 5 μ M, $11.61 \pm 0.23 \mu$ m. $n = 19, 32, 21, 19, 34$. (C) Representative immunofluorescence images of GC-2 spd cells in the control, siCENP-E-1 and siCENP-E-2 groups. The GC-2 spd cells were transfected with the specific siRNA targeting CENP-E for 48 h. DAPI, blue; α -tubulin, green. Scale bar, 10 μ m. (D) Ratios of the cells with chromosome misalignment in the control, siCENP-E-1 and siCENP-E-2 groups. Control, $11.93 \pm 2.32 \%$; siCENP-E-1, $67.88 \pm 1.52 \%$; and siCENP-E-2, $50.55 \pm 8.34 \%$. (E) Ratios of the cells with multinuclei in the control, siCENP-E-1 and siCENP-E-2 groups. Control, $3.13 \pm 0.46 \%$; siCENP-E-1, $8.02 \pm 0.71 \%$; and siCENP-E-2, $4.56 \pm 0.63 \%$. (F) Ratios of the cells with abnormal nucleus, including multinuclei, micronuclei and abnormal nuclear morphology, in the control, siCENP-E-1 and siCENP-E-2 groups. Control, $2.32 \pm 0.37 \%$; siCENP-E-1, $7.83 \pm 0.77 \%$ and siCENP-E-2, $5.69 \pm 0.42 \%$. (G) Ratios of the cells with micronuclei in the control, siCENP-E-1 and siCENP-E-2 groups. Control, $4.89 \pm 0.62 \%$; siCENP-E-1, $10.32 \pm 1.07 \%$ and siCENP-E-2, $6.82 \pm 1.61 \%$. For all graphs, control, $n = 1557$; siCENP-E-1, $n = 1622$; siCENP-E-2, $n = 912$. Group = 4. For all graphs, ANOVA Dunnett's multiple comparisons test. Error bars, mean \pm SEM. ns, $p > 0.05$; *, $p < 0.05$; **, $p < 0.01$; ***, $p < 0.001$; ****, $p < 0.0001$. (For interpretation of the references to colour in this figure legend, the reader is referred to the web version of this article.)

large portion of BubR1 proteins disassociated from the kinetochores and showed an abnormal localization pattern (Fig. 8A-C). In addition, the localization of CDKN1A proteins was also slightly influenced after CENP-E inhibition in the dividing spermatocytes (Fig. 8D, E). Taken together, these results indicate that CENP-E inhibition influences the critical regulators of the spindle assembly checkpoint in meiosis I, which contributes to the disruption of the meiotic spindle assembly checkpoint in primary spermatocytes.

4. Discussion

4.1. Expression patterns of CENP-E in mouse developing testes

In this study, we have revealed that the *CENP-E* gene was highly expressed from 21 days to 28 days after birth, which suggests that CENP-E is essential for the meiosis of spermatocytes. We have found that the high expression level of the *CENP-E* gene remained from 28 to 56 days after birth. Previous studies have revealed that CENP-E proteins initially locate at the centromeres at late diakinesis/early prometaphase I spermatocytes, then localize at the outer kinetochore plate and the fibrous corona of homologous chromosomes at metaphase I spermatocytes, and finally translocate to spindle midzone at anaphase I onset [19,20].

The pattern of the localization of CENP-E in dividing spermatocytes is similar to its localization pattern in mitotic cells, which suggests a potentially conserved role of CENP-E in mitosis and meiosis [20,52,53]. CENP-E proteins were widely expressed in the spermatogonia, the spermatocytes, and the spermatids [22]. The increased intensities of CENP-E at the kinetochores of unaligned bivalents during prometaphase I, and unaligned kinetochores at prometaphase II, suggest that CENP-E might play a role in facilitating kinetochore-microtubule attachment during meiosis [19]. Taken together, these results indicate that CENP-E might play a role in kinetochore-microtubule attachment during the meiotic division of primary spermatocytes.

4.2. CENP-E is essential for kinetochore-microtubule attachment and chromosome alignment in spermatocytes

Due to the essential roles of CENP-E in cell division, *CENP-E* gene knockout results in early embryonic lethality in mice [11], which is an obstacle in the studies of CENP-E in development. The allosteric inhibitor GSK923295 inhibits ATPase activity of the motor domain of CENP-E [17] and mediates a rapid and acute inactivation of CENP-E in cells [54]. Taking advantage of GSK923295, previous studies have demonstrated that CENP-E is essential for end-on kinetochore-microtubule attachment and chromosome congression [55,56]. Thus, in this study, we have established a CENP-E inhibition mouse model using the specific inhibitor GSK923295.

At the molecular level, we have performed quantitative real-time PCR analyses and found that there is no significant difference in the maker genes of early to mid-prophase I, including *Sycp3*, *Rec8*, *Dmc1*, and *Eg5*, between the control and GSK923295 groups. Furthermore, the markers of prophase I *Piwil1* and *CENP-E* were slightly influenced after CENP-E inhibition. In addition, gene transcription levels of *Rfx2*, *Crem*,

and *Sox30* genes were not significantly influenced after CENP-E inhibition. However, *Tnp1* and *Protamine-2* were significantly increased after CENP-E inhibition. Taken together, these results suggest that CENP-E inhibition influences the expression patterns of *Piwil1*, *CENP-E*, *Tnp1*, and *Protamine-2* genes in mouse testes, which may be a consequence of the changes in the populations of spermatogenic cells.

CENP-E is essential for metaphase-to-anaphase transition in mitosis [5]. In mouse oocytes, CENP-E inhibition by antibody injection also results in cell cycle arrest in metaphase I [57]. In this study, we have found that CENP-E inhibition results in prolonged metaphase in primary spermatocytes. GSK923295-mediated CENP-E inhibition leads to a significant increase of dividing spermatocytes I in mouse testes. The Histone H3 (Ser10)-positive spermatocytes in the GSK923295 group suggest prolonged metaphase I and the G₂/M arrest of spermatocytes during meiosis after CENP-E inhibition.

CENP-E transports chromosomes along microtubules in a way independent of microtubule pulling forces [3]. CENP-E and dynein drive the congression of peripheral chromosomes through the balance with arm-ejection forces by chromokinesins [16]. CENP-E controls the stable interactions between depolymerizing microtubule ends and kinetochores [56]. Furthermore, CENP-E converts from a lateral transporter into a microtubule-tip tracker via its motor and tail domain, which is essential for end-on microtubule attachment [56]. Our data suggest that CENP-E mediates homologous chromosome alignment and segregation in the male meiotic division. CENP-E inhibition results in chromosome misalignment, multipolar spindle, and multinuclei in dividing spermatocytes I (Fig. 8F). Taken together, these results indicate that CENP-E is responsible for chromosome alignment and segregation in spermatocytes.

4.3. CENP-E regulates spindle assembly checkpoint and genome stability of spermatocytes

In mitosis, the components of the spindle assembly checkpoint, including Mad1, Mad2, Bub1, BubR1, Bub3, and Mps1 proteins, form a "wait anaphase signal", which inhibits the activation of APC/C (anaphase-promoting complex/cyclosome) and the metaphase-to-anaphase transition [58]. BubR1, a key effector of mitotic checkpoint signaling, associates with Bub3, Mad2, and Cdc20 to form the mitotic checkpoint complex, which suppresses APC/C [59]. BubR1 recruits CENP-E to kinetochores, and the interactions between BubR1 and CENP-E are critical for chromosome alignment [27,28]. Furthermore, CENP-E and BubR1 form a stoichiometric complex, which regulates the status of CENP-E-dependent BubR1 autophosphorylation and the kinase activity of BubR1 [12,28,60]. Taken together, these results indicate that CENP-E functions as a crucial receptor for the silencing of spindle assembly checkpoint after kinetochore-microtubule attachment.

In female meiosis I, CENP-E depletion results in unstable kinetochore-microtubule attachment and the presence of Mad2 at kinetochores, which indicates the activation of spindle assembly checkpoint in mouse oocytes [61]. Meanwhile, CENP-E regulates chromosome bi-orientation and mediates the stability of BubR1 to control metaphase I progression [61]. Our data have shown that CENP-E inhibition results

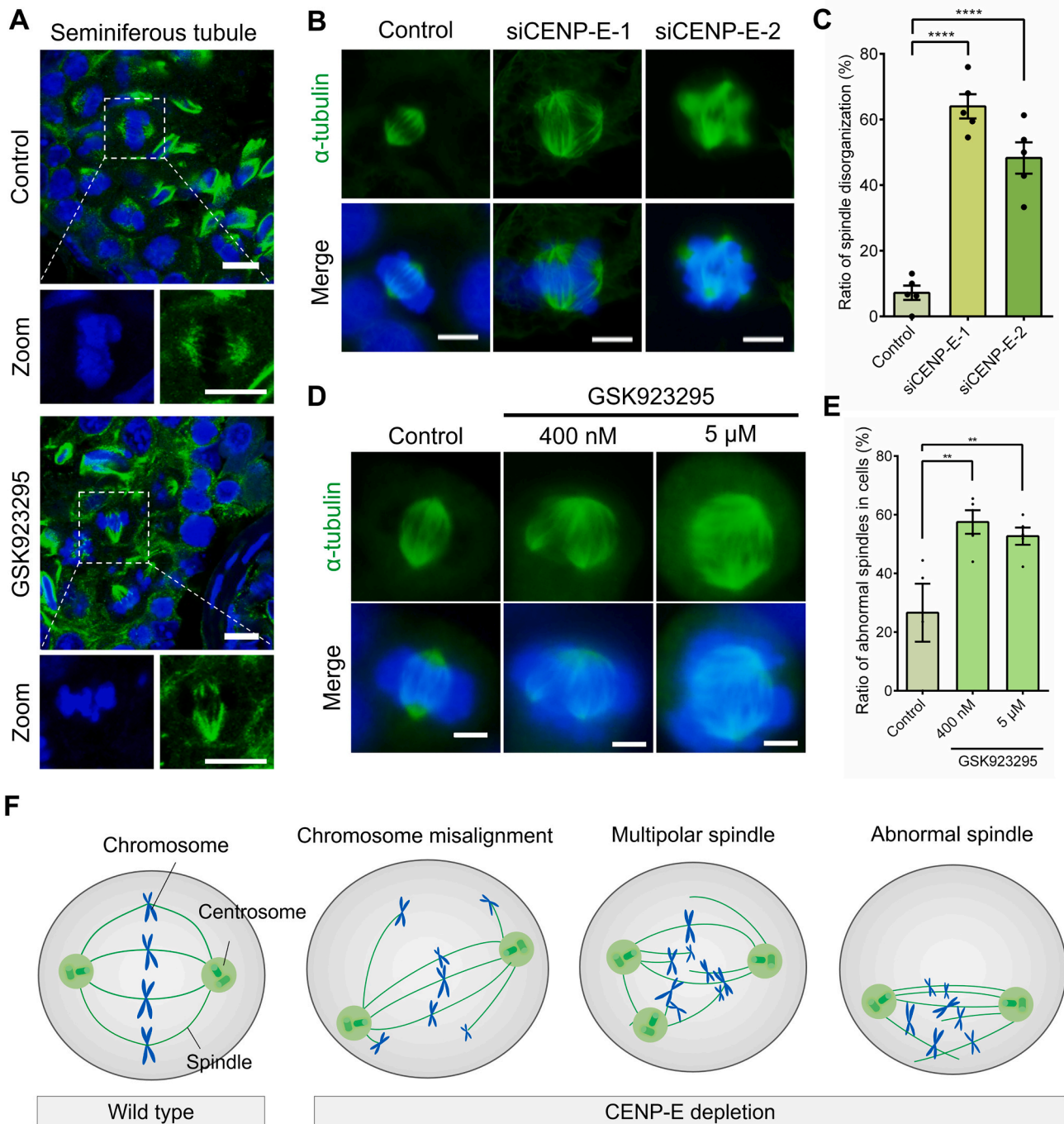


Fig. 6. CENP-E ablation resulted in chromosome misalignment and spindle defects in dividing spermatocytes both *in vivo* and *in vitro*. (A) Immunofluorescence images of spindle microtubules of metaphase I spermatocytes in the control and GSK923295 groups. α -tubulin, green; DAPI, blue. Scale bar, 10 μ m. (B) Representative images of the GC-2 spd cells in the control, siCENP-E-1 and siCENP-E-2 groups. siRNA-mediated CENP-E knockdown resulted in the formation of disorganized spindle and multipolar spindle in the GC-2 spd cells. DAPI, blue; α -tubulin, green. Scale bar, 10 μ m. (C) Ratios of spindle disorganization in the GC-2 spd cells in the control, siCENP-E-1 and siCENP-E-2 groups. Control, 7.19 ± 2.18 %; siCENP-E-1, 64.01 ± 3.70 % and siCENP-E-2, 48.27 ± 4.78 %. For all graphs, control, $n = 1557$; siCENP-E-1, $n = 1622$; siCENP-E-2, $n = 912$. Group = 4. (D) Immunofluorescence images of spindle microtubules in the GC-2 spd cells. Cells were incubated with 400 nM, 1 μ M, 5 μ M and 12.5 μ M GSK923295 for 48 h, respectively. DAPI, blue; α -tubulin, green. Scale bar, 5 μ m. (E) Ratios of abnormal spindles in cells of the control and GSK923295 groups. Control, 26.61 ± 9.90 %, $n = 51$, group = 4; 400 nM, 57.53 ± 4.01 %, $n = 139$, group = 6; 1 μ M, 42.98 ± 5.24 %, $n = 130$, group = 5. (F) Schematic models of the functions and mechanisms of CENP-E in cultured spermatocytes. CENP-E depletion results in chromosome misalignment, multipolar spindle and abnormal spindle in cultured GC-2 spd cells. For all graphs, ANOVA Dunnett's multiple comparisons test. Error bars, mean \pm SEM. **, $p < 0.01$; ****, $p < 0.0001$. (For interpretation of the references to colour in this figure legend, the reader is referred to the web version of this article.)

in the increased expression level of *Cdk1*, *Mad1*, *Mad2*, and *Plk1* genes, which suggests the activation of spindle assembly checkpoint in the male meiotic division. CENP-E inhibition results in the decreased localization of BubR1 proteins at the kinetochores, which indicates CENP-E is

required for the recruitment of BubR1 to the kinetochores and the function of spindle assembly checkpoint during meiosis I. These results demonstrate that loss-of-function of CENP-E in mouse testes activates spindle assembly checkpoint, and then triggers metaphase arrest of

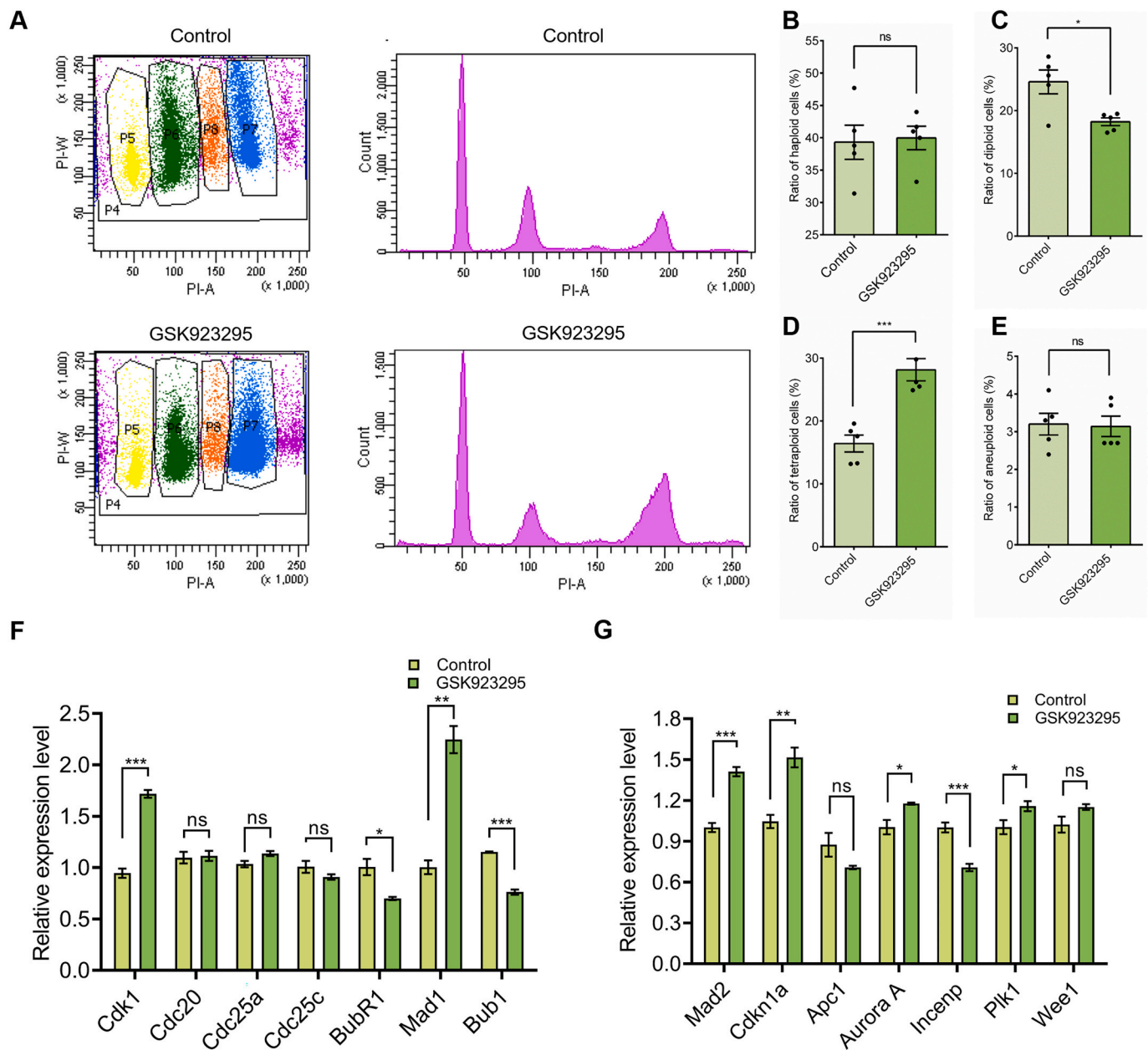


Fig. 7. CENP-E inhibition resulted in the disruption of spermatogenesis and the increase of tetraploid cells. (A) Flow cytometry analyses of the spermatogenic cells in the control and GSK923295 groups. GSK923295 was injected into mouse testes two times every three days at a final concentration of 10 μ M. Analyzed cell numbers: Control, $N = 20,000$; GSK923295, $N = 20,000$. (B) Ratios of the haploid cells in the control and GSK923295 groups. Control, 39.32 ± 2.64 %; GSK923295, 39.98 ± 1.81 %. $N = 5$. (C) Ratios of the diploid cells in the control and GSK923295 group. Control, 16.42 ± 1.33 %; GSK923295, 18.22 ± 0.63 %. $N = 5$. (D) Ratios of the tetraploid cells in the control and GSK923295 groups. Control, 13.07 ± 0.75 %; GSK923295, 19.32 ± 0.92 %. The ratios of aneuploid cells / diploid cells were shown. $N = 5$. (E) Ratios of the aneuploid cells in the control and GSK923295 groups. Control, 3.13 ± 0.25 %; GSK923295, 3.00 ± 0.15 %. (F) Quantitative real-time PCR analyses of expression levels of *Cdk1*, *Cdc20*, *Cdc25a*, *Cdc25c*, *BubR1*, *Mad1*, and *Bub1* genes in the testes of the control and GSK923295 groups. (G) Quantitative real-time PCR analyses of expression levels of *Mad2*, *Cdkn1a*, *Apc1*, *Aurora A*, *Incenp*, *Plk1*, and *Wee1* genes in the testes of the control and GSK923295 groups. Student's *t*-test. Error bars, mean \pm SEM. ns, $p > 0.05$; *, $p < 0.05$; **, $p < 0.01$; ***, $p < 0.001$.

spermatocyte I.

During prometaphase, the recruitment of CENP-E to unattached kinetochores is mediated by Bub1-Bub3 and BubR1-Bub3 complexes [23,62]. In addition, Mad1 recruits CENP-E to the kinetochores for chromosome alignment [63]. Microtubule capture by CENP-E reduces Aurora B-mediated Ndc80 phosphorylation in a tension-independent mechanism [64]. Heterozygous reduction of CENP-E in mice results in the missegregation of a few chromosomes, reduced expression of Mad2, and a low rate of chromosomal instability [11,65,66]. In this study, CENP-E inhibition resulted in defects in the spindle assembly

checkpoint, which is correlated with the increase of aneuploidy cells during meiosis. However, the interactions between CENP-E and spindle assembly checkpoint proteins may be conserved in the meiotic division, which remains to be clarified in future.

The failure in proper chromosome-spindle capture activates the spindle assembly checkpoint, and finally induces mitotic arrest and cell death [17]. Loss-of-function of CENP-E in mitotic cells leads to abnormal metaphase-to-anaphase transition and chromosome missegregation during mitosis [67]. In mammalian cells, CENP-E depletion results in mitotic arrest [25,26]. CENP-E inhibition results in p53-mediated post-

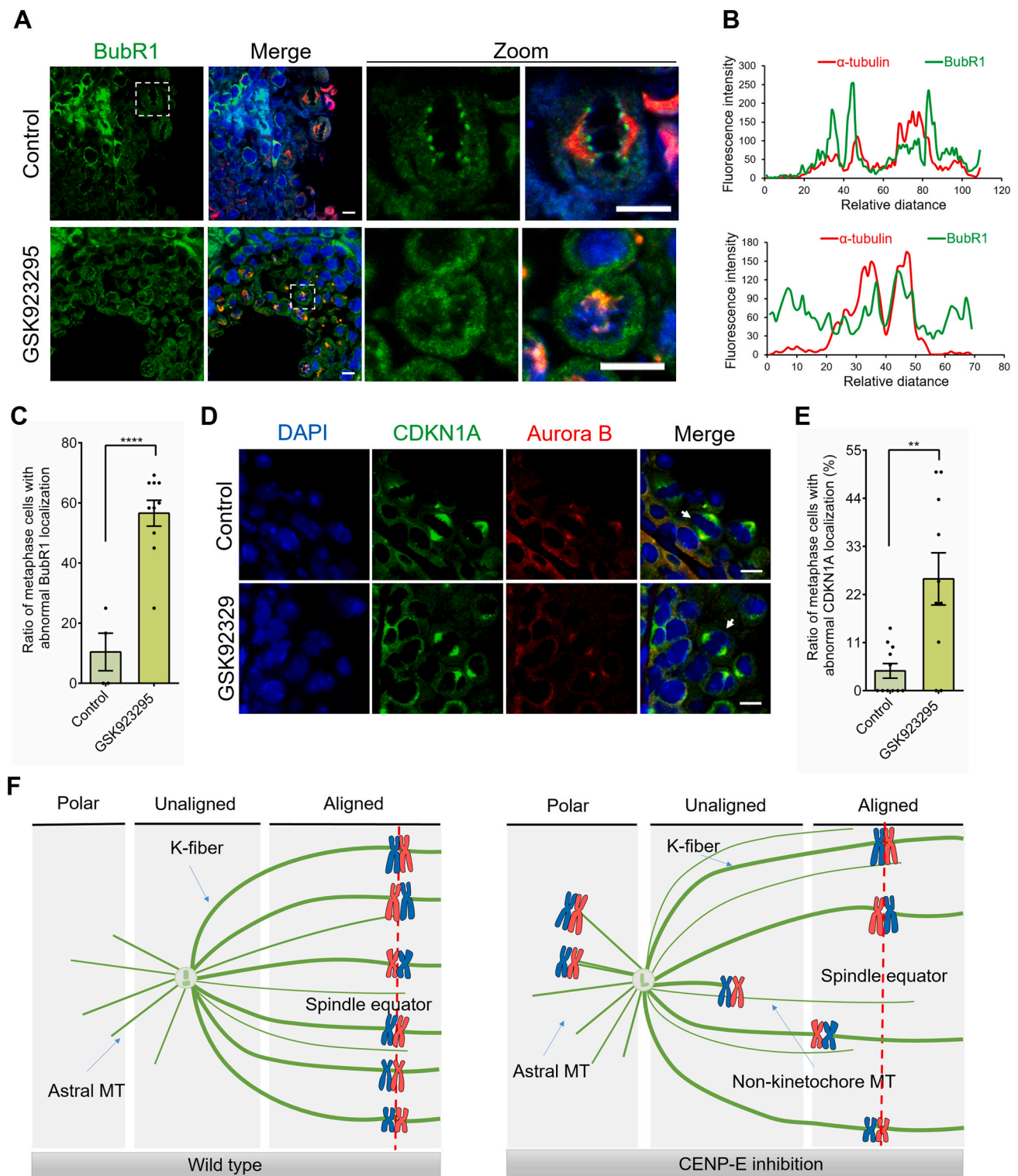


Fig. 8. CENP-E inhibition results in the disruption of the spindle assembly checkpoint in meiosis. (A) Representative immunofluorescence images of BubR1 and α -tubulin in the control and GSK923295 groups. α -tubulin, red; BubR1, green; DAPI, blue. Scale bar, 10 μ m. (B) Line-scan analyses of fluorescent intensities of α -tubulin and BubR1 in metaphase I spermatocytes of the control group and the GSK923295 group. (C) The ratios of metaphase cells with abnormal BubR1 localization in the control and GSK923295 groups. Control, $10.42 \pm 6.25\%$, $N = 4$; GSK923295, $56.59 \pm 4.29\%$, $N = 10$. (D) Representative immunofluorescence images of CDKN1A and Aurora B in the control and GSK923295 groups. (E) The ratios of metaphase cells with abnormal CDKN1A localization in the control and GSK923295 group. Control, $4.51 \pm 1.67\%$, $N = 11$; GSK923295, $25.56 \pm 5.97\%$, $N = 10$. For all graphs, student's t -test. Error bars, mean \pm SEM. **, $p < 0.01$; ****, $p < 0.0001$. (F) Schematic models of the functions of CENP-E in the dividing spermatocytes. CENP-E is required for chromosome alignment and spindle assembly in meiosis. Loss-of-function of CENP-E results in chromosome misalignment, spindle disorganization, and elongated spindle microtubules. (For interpretation of the references to colour in this figure legend, the reader is referred to the web version of this article.)

mitotic apoptosis and aneuploidy-associated DNA damage response induced by chromosome missegregation [68]. Furthermore, spindle malfunctioning leads to prolonged mitotic arrest and cell death [69]. However, we found that CENP-E inhibition did not result in obvious cell apoptosis in mouse testes, which may be caused by the complex internal environment in the testes or the shedding of dead cells into the epididymis.

4.4. CENP-E regulates spindle length and organization in meiosis

In different cell types, the mitotic metaphase spindle remains at a steady-state length, which is regulated by microtubule dynamics, molecular forces, and motor proteins [70–75]. It is well known that kinesin-14 and kinesin-5 are key regulators in the maintenance of the length and structure of the mitotic spindle through the push and pull mechanism [75–78]. However, the roles of kinesin-7 CENP-E in spindle assembly remain largely unknown. In this study, we have found that the length of spindle microtubules was $9.71 \pm 0.16 \mu\text{m}$ in the GSK923295 group compared with $8.48 \pm 0.17 \mu\text{m}$ in the control group in metaphase spermatocytes. Our results have shown that the spindle length was increased after CENP-E inhibition in metaphase I spermatocytes. Inconsistent with this result, CENP-E inhibition also results in the elongation of the mitotic spindle in cultured GC-2 spd cells. Meanwhile, spindle length is positively correlated with the degree of CENP-E inhibition.

CENP-E is a slow microtubule plus-end-direct motor, which promotes microtubule plus-end elongation *in vitro* [79]. In Hec1 and CENP-E co-depleted cells, the kinetochore to spindle pole distance becomes longer compared with Hec1-depleted cells [80], which suggests that CENP-E suppresses chromosome motion toward the spindle equator. A recent study suggests that CENP-E is the predominant driver of microtubule flux from prometaphase to metaphase [81]. The motor activity of CENP-E is essential for microtubule flux before the kinetochore-microtubule attachment. The localization of CENP-E at kinetochore fibers during metaphase [3–5] and antiparallel microtubule of midzone during anaphase [5] indicates its roles in kinetochore-microtubule attachment. Furthermore, the localization of CENP-E at interpolar microtubules suggests that CENP-E interacts with antiparallel interpolar microtubules and mediates microtubule sliding [81]. CENP-E cooperates with kinesin-5 Eg5 and KIF15 to regulate microtubule flux and spindle length by counteracting kinesin-13 MCAK-dependent microtubule depolymerization [81]. Taken together, CENP-E is an emerging regulator of spindle length and spindle organization in both mitosis and meiosis.

CENP-E depletion results in a 50 % reduction in microtubule numbers on congressed chromosomes in mitotic cells [11,82]. In addition, CENP-E deletion led to pericentriolar material fragmentation, centrosome destabilization, shorten astral microtubules, and oblique cell division [83]. In this study, we have shown that there is a significant decrease in PRC1-labelled microtubules in metaphase I spermatocytes. Our results indicate that CENP-E is responsible for the organization of the meiotic spindle in dividing spermatocytes *in vivo*. Previous studies have suggested that CENP-E contains a microtubule-binding site at the motor domain and an ATP-independent microtubule-binding site at the tail domain, which is required for the crosslinking of parallel or antiparallel microtubules in cells [84]. The microtubule crosslinking ability of CENP-E might play a role in spindle assembly during cell division, which requires further investigation in future.

5. Conclusions

In conclusion, we have revealed that CENP-E inhibition results in chromosome misalignment and metaphase arrest in dividing spermatocytes during meiosis. CENP-E inhibition activates the spindle assembly checkpoint in meiosis, which contributes to the cell cycle arrest of spermatocytes at metaphase I. Furthermore, CENP-E depletion leads

to chromosome missegregation in spermatocytes and the increase of tetraploid cells in seminiferous tubules. In addition, we have found that CENP-E inhibition results in spindle elongation of spermatocytes in metaphase I, which suggests the essential roles of CENP-E in spindle assembly in meiosis. Taken together, our data indicate that CENP-E regulates spindle assembly and chromosome alignment in dividing spermatocytes during male meiotic division.

Transparency document

The Transparency document associated with this article can be found, in the online version.

CRediT authorship contribution statement

Zhen-Yu She: Conceptualization, Data curation, Formal analysis, Funding acquisition, Investigation, Project administration, Resources, Supervision, Validation, Visualization, Writing – original draft, Writing – review & editing. **Meng-Fei Xu:** Formal analysis, Investigation, Validation, Visualization, Writing – original draft. **Sun-Ying Jiang:** Formal analysis, Writing – original draft. **Ya-Lan Wei:** Formal analysis, Validation, Writing – original draft, Writing – review & editing.

Declaration of competing interest

The authors declare that they have no known competing financial interests or personal relationships that could have appeared to influence the work reported in this paper.

Acknowledgments

We thank all members of the Cytoskeleton Laboratory at Fujian Medical University for helpful discussions. We thank Si-Yi Zheng, Ying Lin, Qi Ke, and Jun Song at Experimental Teaching Center of Basic Medical Sciences at Fujian Medical University for their support. We thank Min-Xia Wu, Lin-Ying Zhou, Xi Lin, Jun-Jin Lin, and Zhi-Hong Huang at Public Technology Service Center, Fujian Medical University for technical assistance. This study was supported by the following grants: National Natural Science Foundation of China (grant number 82001608), Natural Science Foundation of Fujian Province, China (grant number 2019J05071), Fujian Provincial Health Technology Project (grant number 2018-1-69), and Fujian Medical University high level talents scientific research start-up funding project (grant number XRCZX2017025).

Appendix A. Supplementary data

Supplementary data to this article can be found online at <https://doi.org/10.1016/j.bbamcr.2022.119306>.

References

- [1] S.I. Nagaoka, T.J. Hassold, P.A. Hunt, Human aneuploidy: mechanisms and new insights into an age-old problem, *Nat Rev Genet* 13 (2012) 493–504.
- [2] Y. Wu, X. Hu, Z. Li, M. Wang, S. Li, X. Wang, X. Lin, S. Liao, Z. Zhang, X. Feng, S. Wang, X. Cui, et al., Transcription factor RFX2 is a key regulator of mouse spermiogenesis, *Sci. Rep.* 6 (2016) 20435.
- [3] T.M. Kapoor, M.A. Lampson, P. Hergert, L. Cameron, D. Cimini, E.D. Salmon, B. F. McEwen, A. Khodjakov, Chromosomes can congress to the metaphase plate before biorientation, *Science* 311 (2006) 388–391.
- [4] K.W. Wood, R. Sakowicz, L.S. Goldstein, D.W. Cleveland, CENP-E is a plus end-directed kinetochore motor required for metaphase chromosome alignment, *Cell* 91 (1997) 357–366.
- [5] T.J. Yen, D.A. Compton, D. Wise, R.P. Zinkowski, B.R. Brinkley, W.C. Earnshaw, D. W. Cleveland, CENP-E, a novel human centromere-associated protein required for progression from metaphase to anaphase, *EMBO J.* 10 (1991) 1245–1254.
- [6] K.W. Yu, N. Zhong, Y. Xiao, Z.Y. She, Mechanisms of kinesin-7 CENP-E in kinetochore-microtubule capture and chromosome alignment during cell division, *Biol. Cell.* 111 (2019) 143–160.

- [7] C.A. Cooke, B. Schaar, T.J. Yen, W.C. Earnshaw, Localization of CENP-E in the fibrous corona and outer plate of mammalian kinetochores from prometaphase through anaphase, *Chromosoma* 106 (1997) 446–455.
- [8] X. Yao, K.L. Anderson, D.W. Cleveland, The microtubule-dependent motor centromere-associated protein E (CENP-E) is an integral component of kinetochore corona fibers that link centromeres to spindle microtubules, *J. Cell Biol.* 139 (1997) 435–447.
- [9] D. Liu, X. Ding, J. Du, X. Cai, Y. Huang, T. Ward, A. Shaw, Y. Yang, R. Hu, C. Jin, X. Yao, Human NUF2 interacts with centromere-associated protein E and is essential for a stable spindle microtubule-kinetochore attachment, *J. Biol. Chem.* 282 (2007) 21415–21424.
- [10] L. Tovini, S.E. McClelland, Impaired CENP-E function renders large chromosomes more vulnerable to congression failure, *Biomolecules* 9 (2019) 44.
- [11] F.R. Putkey, T. Cramer, M.K. Morphey, A.D. Silk, R.S. Johnson, J.R. McIntosh, D. W. Cleveland, Unstable kinetochore-microtubule capture and chromosomal instability following deletion of CENP-E, *Dev. Cell* 3 (2002) 351–365.
- [12] B.A. Weaver, Z.Q. Bonday, F.R. Putkey, G.J. Kops, A.D. Silk, D.W. Cleveland, Centromere-associated protein-E is essential for the mammalian mitotic checkpoint to prevent aneuploidy due to single chromosome loss, *J. Cell Biol.* 162 (2003) 551–563.
- [13] M. Tanudji, J. Shoemaker, L. L'Italien, L. Russell, G. Chin, X.M. Schebye, Gene silencing of CENP-E by small interfering RNA in HeLa cells leads to missegregation of chromosomes after a mitotic delay, *Mol. Biol. Cell* 15 (2004) 3771–3781.
- [14] L. Veneziano, V. Barra, D. Cilluffo, A. Di Leonardo, Proliferation of aneuploid cells induced by CENP-E depletion is counteracted by the p14ARF tumor suppressor, *Mol. Gen. Genomics* 294 (2019) 149–158.
- [15] C.P. Yang, L. Liu, A.E. Ikui, S.B. Horwitz, The interaction between mitotic checkpoint proteins, CENP-E and BubR1, is diminished in epothilone B-resistant A549 cells, *Cell Cycle* 9 (2010) 1207–1213.
- [16] M. Barisic, P. Aguiar, S. Geley, H. Maiato, Kinetochore motors drive congression of peripheral polar chromosomes by overcoming random arm-ejection forces, *Nat. Cell Biol.* 16 (2014) 1249–1256.
- [17] K.W. Wood, L. Lad, L. Luo, X. Qian, S.D. Knight, N. Nevins, K. Brejc, D. Sutton, A. G. Gilmartin, P.R. Chua, R. Desai, S.P. Schauer, et al., Antitumor activity of an allosteric inhibitor of centromere-associated protein-E, *Proc. Natl. Acad. Sci. U. S. A.* 107 (2010) 5839–5844.
- [18] R. Pisa, D.Y.Z. Phua, T.M. Kapoor, Distinct mechanisms of resistance to a CENP-E inhibitor emerge in near-haploid and diploid cancer cells, *Cell Chem Biol* 27 (2020) 850–857.e6.
- [19] M.T. Parra, J. Page, T.J. Yen, D. He, A. Valdeolmillos, J.S. Rufas, J.A. Suja, Expression and behaviour of CENP-E at kinetochores during mouse spermatogenesis, *Chromosoma* 111 (2002) 53–61.
- [20] M. Kallio, T. Mustalahti, T.J. Yen, J. Lähdeite, Immunolocalization of alpha-tubulin, gamma-tubulin, and CENP-E in male rat and male mouse meiotic divisions: pathway of meiosis I spindle formation in mammalian spermatocytes, *Dev. Biol.* 195 (1998) 29–37.
- [21] M.T. Parra, R. Gómez, A. Viera, E. Llano, A.M. Pendás, J.S. Rufas, J.A. Suja, Sequential assembly of centromeric proteins in male mouse meiosis, *PLoS Genet.* 5 (2009), e1000417.
- [22] Z.Y. She, K.W. Yu, N. Zhong, Y. Xiao, Y.L. Wei, Y. Lin, Y.L. Li, M.H. Lu, Kinesin-7 CENP-E regulates chromosome alignment and genome stability of spermatogenic cells, *Cell Death Discov* 6 (2020) 25.
- [23] X.D. Zhang, J. Goeres, H. Zhang, T.J. Yen, A.C. Porter, M.J. Matunis, SUMO-2/3 modification and binding regulate the association of CENP-E with kinetochores and progression through mitosis, *Mol. Cell* 29 (2008) 729–741.
- [24] G.K. Chan, S.A. Jablonski, V. Sudakin, J.C. Hittle, T.J. Yen, Human BUBR1 is a mitotic checkpoint kinase that monitors CENP-E functions at kinetochores and binds the cyclosome/APC, *J. Cell Biol.* 146 (1999) 941–954.
- [25] X. Yao, A. Abrieu, Y. Zheng, K.F. Sullivan, D.W. Cleveland, CENP-E forms a link between attachment of spindle microtubules to kinetochores and the mitotic checkpoint, *Nat. Cell Biol.* 2 (2000) 484–491.
- [26] A. Abrieu, J.A. Kahana, K.W. Wood, D.W. Cleveland, CENP-E as an essential component of the mitotic checkpoint in vitro, *Cell* 102 (2000) 817–826.
- [27] T. Legal, D. Hayward, A. Gluszek-Kustusz, E.A. Blackburn, C. Spanos, J. Rappsilber, U. Grunberg, J.P.I. Welburn, The C-terminal helix of BubR1 is essential for CENP-E-dependent chromosome alignment, *J. Cell Sci.* 133 (jcs246025) (2020).
- [28] Y. Mao, A. Abrieu, D.W. Cleveland, Activating and silencing the mitotic checkpoint through CENP-E-dependent activation/inactivation of BubR1, *Cell* 114 (2003) 87–98.
- [29] X. Qian, A. McDonald, H.J. Zhou, N.D. Adams, C.A. Parrish, K.J. Duffy, D.M. Fitch, R. Tedesco, L.W. Ashcraft, B. Yao, et al., Discovery of the first potent and selective inhibitor of centromere-associated protein E: GSK923295, *ACS Med. Chem. Lett.* 1 (2010) 30–34.
- [30] V. Chung, E.I. Heath, W.R. Schelman, B.M. Johnson, L.C. Kirby, K.M. Lynch, J. D. Botbyl, T.A. Lampkin, K.D. Holen, First-time-in-human study of GSK923295, a novel antimetastatic inhibitor of centromere-associated protein E (CENP-E), in patients with refractory cancer, *Cancer Chemother. Pharmacol.* 69 (2012) 733–741.
- [31] R.B. Lock, H. Carol, C.L. Morton, S.T. Keir, C.P. Reynolds, M.H. Kang, J.M. Maris, A.W. Wozniak, R. Gorlick, E.A. Kolb, P.J. Houghton, M.A. Smith, Initial testing of the CENP-E inhibitor GSK923295A by the pediatric preclinical testing program, *Pediatr. Blood Cancer* 58 (2012) 916–923.
- [32] S.O. Tcherniuk, A.V. Oleinikov, Pgp efflux pump decreases the cytostatic effect of CENP-E inhibitor GSK923295, *Cancer Lett.* 361 (2015) 97–103.
- [33] Z.Y. She, N. Zhong, K.W. Yu, Y. Xiao, Y.L. Wei, Y. Lin, Y.L. Li, M.H. Lu, Kinesin-5 Eg5 is essential for spindle assembly and chromosome alignment of mouse spermatocytes, *Cell Div* 15 (2020) 6.
- [34] C.P. Leblond, Y. Clermont, Definition of the stages of the cycle of the seminiferous epithelium in the rat, *Ann. N. Y. Acad. Sci.* 55 (1952) 548–573.
- [35] C.P. Leblond, Y. Clermont, Spermiogenesis of rat, mouse, hamster and guinea pig as revealed by the periodic acid-fuchsin sulfuric acid technique, *Am. J. Anat.* 195; 90:167–215.
- [36] L.D. Russell, R.A. Ettlin, A.P.S. Hikim, E.D. Clegg, in: *Histological and Histopathological Evaluation of the Testis*, Cache River Press, Florida, 1990, pp. 119–162.
- [37] D.H. Castrillon, B.J. Quade, T.Y. Wang, C. Quigley, C.P. Crum, The human VASA gene is specifically expressed in the germ cell lineage, *Proc. Natl. Acad. Sci. U. S. A.* 97 (2000) 9585–9590.
- [38] S. Kuramochi-Miyagawa, T. Watanabe, K. Gotoh, K. Takamatsu, S. Chuma, K. Kojima-Kita, Y. Shiromoto, N. Asada, A. Toyoda, A. Fujiyama, Y. Totoki, T. Shibata, et al., MVH in piRNA processing and gene silencing of retrotransposons, *Genes Dev.* 24 (2010) 887–892.
- [39] L. Yuan, J.G. Liu, J. Zhao, E. Brundell, B. Daneholt, C. Höög, The murine SCP3 gene is required for synaptonemal complex assembly, chromosome synapsis, and male fertility, *Mol. Cell* 5 (2000) 73–83.
- [40] Y. Watanabe, P. Nurse, Cohesin Rec8 is required for reductional chromosome segregation at meiosis, *Nature* 400 (1999) 461–464.
- [41] H. Xu, M.D. Beasley, W.D. Warren, G.T. van der Horst, M.J. McKay, Absence of mouse REC8 cohesin promotes synapsis of sister chromatids in meiosis, *Dev. Cell* 8 (2005) 949–961.
- [42] E. Dray, M.H. Dunlop, L. Kauppi, J. San Filippo, C. Wiese, M.S. Tsai, S. Begovic, D. Schild, M. Jasin, S. Keeney, P. Sung, Molecular basis for enhancement of the meiotic DMC1 recombinase by RAD51 associated protein 1 (RAD51AP1), *Proc. Natl. Acad. Sci. U. S. A.* 108 (2011) 3560–3565.
- [43] C. Krausz, P. Sassone-Corsi, Genetic control of spermiogenesis: insights from the CREM gene and implications for human infertility, *Reprod. BioMed. Online* 10 (2005) 64–71.
- [44] C.A. Feng, C. Spiller, D.J. Merriner, M.K. O'Bryan, J. Bowles, P. Koopman, SOX30 is required for male fertility in mice, *Sci. Rep.* 7 (2017) 17619.
- [45] P. Mali, A. Kaipia, M. Kangasniemi, J. Toppari, M. Sandberg, N.B. Hecht, M. Parvinen, Stage-specific expression of nucleoprotein mRNAs during rat and mouse spermiogenesis, *Reprod. Fert. Dev.* 1 (1989) 369–382.
- [46] C. Cho, H. Jung-Ha, W.D. Willis, E.H. Goulding, P. Stein, Z. Xu, R.M. Schultz, N. B. Hecht, E.M. Eddy, Protamine 2 deficiency leads to sperm DNA damage and embryonic death in mice, *Biol. Reprod.* 69 (2003) 211–217.
- [47] R.J. Botelho, L. DiNicolo, N. Tsao, A. Karaiskakis, M. Tarsounas, P.B. Moens, R. E. Pearlman, The genomic structure of SYCP3, a meiosis-specific gene encoding a protein of the chromosome core, *Biochim. Biophys. Acta* 1518 (2001) 294–299.
- [48] C.G. Bisig, M.F. Guiraldelli, A. Kouznetsova, H. Scherthan, C. Höög, D.S. Dawson, R.J. Pezza, Synaptonemal complex components present at centromeres and are required for homologous centromere pairing in mouse spermatocytes, *PLoS Genet.* 8 (2012), e1002701.
- [49] M.J. Wolkowicz, S.A. Coonrod, P.P. Reddi, J.L. Millan, M.C. Hofmann, J.C. Herr, Refinement of the differentiated phenotype of the spermatogenic cell line GC-2spd (ts), *Biol. Reprod.* 55 (1996) 923–932.
- [50] M.C. Hofmann, R.A. Hess, E. Goldberg, J.L. Millán, Immortalized germ cells undergo meiosis in vitro, *Proc. Natl. Acad. Sci. U. S. A.* 91 (1994) 5533–5537.
- [51] P. Verma, P. Parte, Revisiting the characteristics of testicular germ cell lines GC-1 (spg) and GC-2(spd)ts, *Mol. Biotechnol.* 63 (2021) 941–952.
- [52] T.J. Yen, G. Li, B.T. Schaar, I. Szilak, D.W. Cleveland, CENP-E is a putative kinetochore motor that accumulates just before mitosis, *Nature* 359 (1992) 536–539.
- [53] V.A. Lombillo, C. Nislow, T.J. Yen, V.I. Gelfand, J.R. McIntosh, Antibodies to the kinesin motor domain and CENP-E inhibit microtubule depolymerization-dependent motion of chromosomes in vitro, *J. Cell Biol.* 128 (1995) 107–115.
- [54] B. Craske, J.P.I. Welburn, Leaving no-one behind: how CENP-E facilitates chromosome alignment, *Essays Biochem.* 64 (2020) 313–324.
- [55] V. Sikirzhyski, F. Renda, I. Tikhonenko, V. Magidson, B.F. McEwen, A. Khodjakov, Microtubules assemble near most kinetochores during early prometaphase in human cells, *J. Cell Biol.* 217 (2018) 2647–2659.
- [56] N. Gudimchuk, B. Vitre, Y. Kim, A. Kiyatkin, D.W. Cleveland, F.I. Ataullakhanov, E. L. Grishchuk, Kinetochore kinesin CENP-E is a processive bi-directional tracker of dynamic microtubule tips, *Nat. Cell Biol.* 15 (2013) 1079–1088.
- [57] N.S. Duesbery, T. Choi, K.D. Brown, K.W. Wood, J. Resau, K. Fukasawa, D. W. Cleveland, G.F. Vande Woude, CENP-E is an essential kinetochore motor in maturing oocytes and is masked during Mos-dependent, cell cycle arrest at metaphase II, *Proc. Natl. Acad. Sci. U. S. A.* 94 (1997) 9165–9170.
- [58] A. Musacchio, E.D. Salmon, The spindle-assembly checkpoint in space and time, *Nat Rev Mol Cell Biol* 8 (2007) 379–393.
- [59] V. Sudakin, G.K. Chan, T.J. Yen, Checkpoint inhibition of the APC/C in HeLa cells is mediated by a complex of BUBR1, BUB3, CDC20, and MAD2, *J. Cell Biol.* 154 (2001) 925–936.
- [60] Y. Guo, C. Kim, S. Ahmad, J. Zhang, Y. Mao, CENP-E-dependent BubR1 autophosphorylation enhances chromosome alignment and the mitotic checkpoint, *J. Cell Biol.* 198 (2012) 205–217.
- [61] L. Gui, H. Homer, Spindle assembly checkpoint signalling is uncoupled from chromosomal position in mouse oocytes, *Development* 139 (2012) 1941–1946.
- [62] V.L. Johnson, M.I. Scott, S.V. Holt, D. Hussein, S.S. Taylor, Bub1 is required for kinetochore localization of BubR1, Cenp-E, Cenp-F and Mad2, and chromosome congression, *J. Cell Sci.* 117 (2004) 1577–1589.

- [63] T. Akera, Y. Goto, M. Sato, M. Yamamoto, Y. Watanabe, Mad1 promotes chromosome congression by anchoring a kinesin motor to the kinetochore, *Nat. Cell Biol.* 17 (2015) 1124–1133.
- [64] C. Taveras, C. Liu, Y. Mao, A tension-independent mechanism reduces Aurora B-mediated phosphorylation upon microtubule capture by CENP-E at the kinetochore, *Cell Cycle* 18 (2019) 1349–1363.
- [65] B.A. Weaver, A.D. Silk, C. Montagna, P. Verdier-Pinard, D.W. Cleveland, Aneuploidy acts both oncogenically and as a tumor suppressor, *Cancer Cell* 11 (2007) 25–36.
- [66] A.D. Silk, L.M. Zasadil, A.J. Holland, B. Vitre, D.W. Cleveland, B.A. Weaver, Chromosome missegregation rate predicts whether aneuploidy will promote or suppress tumors, *Proc. Natl. Acad. Sci. U. S. A.* 110 (2013) E4134–E4141.
- [67] X. Liu, L. Xu, J. Li, P.Y. Yao, W. Wang, H. Ismail, H. Wang, B. Liao, Z. Yang, T. Ward, K. Ruan, J. Zhang, et al., Mitotic motor CENP-E cooperates with PRC1 in temporal control of central spindle assembly, *J. Mol. Cell Biol.* 12 (2020) 654–665.
- [68] A. Ohashi, M. Otori, K. Iwai, Y. Nakayama, T. Nambu, D. Morishita, T. Kawamoto, M. Miyamoto, T. Hirayama, M. Okaniwa, H. Banno, T. Ishikawa, et al., Aneuploidy generates proteotoxic stress and DNA damage concurrently with p53-mediated post-mitotic apoptosis in SAC-impaired cells, *Nat. Commun.* 6 (2015) 7668.
- [69] N.N. Mafy, K. Matsuo, S. Hiruma, R. Uehara, N. Tamaoki, Photoswitchable CENP-E inhibitor enabling the dynamic control of chromosome movement and mitotic progression, *J. Am. Chem. Soc.* 142 (2020) 1763–1767.
- [70] G. Goshima, R. Wollman, N. Stuurman, J.M. Scholey, R.D. Vale, Length control of the metaphase spindle, *Curr. Biol.* 15 (2005) 1979–1988.
- [71] A. Chakravarty, L. Howard, D.A. Compton, A mechanistic model for the organization of microtubule asters by motor and non-motor proteins in a mammalian mitotic extract, *Mol. Biol. Cell* 15 (2004) 2116–2132.
- [72] K.S. Burbank, T.J. Mitchison, D.S. Fisher, Slide-and-cluster models for spindle assembly, *Curr. Biol.* 17 (2007) 1373–1383.
- [73] S. Dumont, T.J. Mitchison, Force and length in the mitotic spindle, *Curr. Biol.* 19 (2009) R749–R761.
- [74] S. Cai, L.N. Weaver, S.C. Ems-McClung, C.E. Walczak, Kinesin-14 family proteins HSET/XCTK2 control spindle length by cross-linking and sliding microtubules, *Mol. Biol. Cell* 20 (2009) 1348–1359.
- [75] Z.Y. She, W.X. Yang, Molecular mechanisms of kinesin-14 motors in spindle assembly and chromosome segregation, *J. Cell Sci.* 130 (2017) 2097–2110.
- [76] L.C. Kapitein, E.J. Peterman, B.H. Kwok, J.H. Kim, T.M. Kapoor, C.F. Schmidt, The bipolar mitotic kinesin Eg5 moves on both microtubules that it crosslinks, *Nature* 435 (2005) 114–118.
- [77] C.E. Walczak, R. Heald, Mechanisms of mitotic spindle assembly and function, *Int. Rev. Cytol.* 265 (2008) 111–158.
- [78] S.M. van den Wildenberg, L. Tao, L.C. Kapitein, C.F. Schmidt, J.M. Scholey, E. J. Peterman, The homotetrameric kinesin-5 KLP61F preferentially crosslinks microtubules into antiparallel orientations, *Curr. Biol.* 18 (2008) 1860–1864.
- [79] H.S. Sardar, V.G. Luczak, M.M. Lopez, B.C. Lister, S.P. Gilbert, Mitotic kinesin CENP-E promotes microtubule plus-end elongation, *Curr. Biol.* 20 (2010) 1648–1653.
- [80] K. Iemura, K. Tanaka, Chromokinesin kid and kinetochore kinesin CENP-E differentially support chromosome congression without end-on attachment to microtubules, *Nat. Commun.* 6 (2015) 6447.
- [81] Y. Steblyanko, G. Rajendraprasad, M. Osswald, S. Eibes, A. Jacome, S. Geley, A. J. Pereira, H. Maiato, M. Barisic, Microtubule poleward flux in human cells is driven by the coordinated action of four kinesins, *EMBO J.* 39 (2020), e105432.
- [82] B.F. McEwen, G.K. Chan, B. Zubrowski, M.S. Savoian, M.T. Sauer, T.J. Yen, CENP-E is essential for reliable bioriented spindle attachment, but chromosome alignment can be achieved via redundant mechanisms in mammalian cells, *Mol. Biol. Cell* 12 (2001) 2776–2789.
- [83] M. Owa, B. Dynlacht, A non-canonical function for centromere-associated protein-E controls centrosome integrity and orientation of cell division, *Commun Biol* 4 (2021) 358.
- [84] H. Liao, G. Li, T.J. Yen, Mitotic regulation of microtubule cross-linking activity of CENP-E kinetochore protein, *Science* 265 (1994) 394–398.